Chapter 4

Application to laboratory data

In order to check the main theoretically derived results of the stress sensitivity of porous rock I applied the stress sensitivity approach to velocity vs. stress observations from isotropic as well as anisotropic rocks. Hereby, main intention was to investigate, if there are rocks where the stress sensitivity tensor has only one independent entry. If such rocks are isostatically loaded the fit parameter $D = \theta_c/K_{\mathrm{dryS}}$ should be a universal quantity for all properties of a given rock that depend mainly on the porosity and geometry of the pore space.

In the case of isotropic rocks these properties are the elastic moduli as well as P- and S-wave velocity. In fact, I will show that there are many rocks with an approximatly isotropic stress sensitivity tensor. Moreover, I found that there are isotropic low porosity crystalline rocks where the universality of D is even valid for the electrical resitivity.

If D is a universal quantity of a given rock and the rock is isostatically loaded its anisotropy does not change with load. Then, Thomsen's and Tsvankin's anisotropy parameter, in the case of TI and orthorhombic media, respectively, should be independent from the applied load. I will show that there are sedimentary as well as highly metamorphic anisotropic rocks where parameter D is universal for all velocities in all directions and where the anisotropy parameters are at least approximately constant.

4.1 General remarks on fit procedure

For any stress dependent property under consideration the fit procedure is a two-step process. This is imposed by the postulated universality of parameter D. Again, the basic fit equation in terms of, e.g., P- and S-wave velocity, looks like:

$$V_P(\mathrm{P_{eff}}) = A_P + K_P\mathrm{P_{eff}} - B_P \exp(-D_P\mathrm{P_{eff}}) \quad (4.1)$$

$$V_S(\mathrm{P_{eff}}) = A_S + K_S\mathrm{P_{eff}} - B_S \exp(-D_S\mathrm{P_{eff}}) \quad (4.2)$$

Fitting the equation to the data is done by means of a least-squares fit. In general, this means, that a certain set of parameters is searched for, that leads to the minimal deviation of the fit equation from the observed data. The squared sum of the deviation

is frequently denoted as χ^2. Basically, χ^2 reads (e.g., Press *et al.*, 2002)

$$\chi^2 = \sum_{i=0}^{N-1} \left[\frac{y_i - y(x_i, a_0 ... a_{M-1})}{\sigma_i} \right]^2 , \tag{4.3}$$

where N is the number of observed data y_i, and $y(x_i, a_0 ... a_{M-1})$ are the values of the assumed model with M adjustable parameters a_j (j = 0,..., M - 1). χ^2 is dimensionless since σ_i is the standard deviation of the observed value y_i. If σ_i is not known for the considered data set a default value of 1 is usually assumed.

However, the fit equation used here, e.g., eq. (4.1), is not linear in its fit parameters and cannot usefully be linearized. Thus, the fit procedure must be conducted iteratively. Here, the Levenberg-Marquardt Method (see, e.g., chapter 15, pp. 688 of Press *et al.*, 2002, for details) was used for this purpose, provided by the MATLAB software package. It turned out that it is necessary to fit velocities in km/s, and moduli in GPa to avoid instabilities in the fit process due to numerical limitations.

A non-linear least squares fit requires the definition of initial values for the searched for fit parameters. The fit procedure is highly sensitive to the initial guess for parameter A. It was found empirically that A should be of the order of 90 to 95% of the maximum value in the data. This order of magnitude usually corresponds to transition zone from non-linear increase at low applied stress to linear increase for higher stress. In the case of 176 velocity data sets from Freund (1992) it was possible to fit all 88 P- and corresponding S-wave velocities completely automized by calculating the initial value A to 95% of the maximum velocity of the certain P- and S-wave.

In general, the application of an iterative model optimization is fraught with problems. On the one hand site it is possible that the solution does not converge. Additionally, it is possible that the solution converges at a local minimum of χ^2. Consequently, the obtained set of best fit parameters does not represent the searched for parameters. However, the stress sensitivity approach has the advantage of knowing the physical meaning of the certain fit parameters. Thus, convergence in a local minimum can easily be identified if the fit parameters show non-physical values.

In the first step, eq. (4.1) and (4.2) are used to fit the corresponding data for a given set of initial fit values. This gives a first set of best fit parameters A_P, K_P, B_P, D_P and A_S, K_S, B_S, D_S. In the case of isostatic load and an isotropic stress sensitivity tensor $D = D_P = D_S$ should be valid.

In the second step parameter D is calculated as the mean of D_P and D_S. Then, the data are refitted but now with a common and constant D. This definition of a constant D makes the fit equation linear in its fit parameters and, hence, the second fit can be conducted as a linear least squares fit.

The second step improves the quality of the fit in many cases, especially for rocks, where D_P and D_S obtained from the first fit show a high degree of correspondence. There are also rocks, where this procedure decreases the quality of the fit. However, even for those rocks it was, in general, possible to fit the data quite well. The work flow of the two step fit procedure is schematically illustrated in Fig. (4.1).

Figure 4.2 shows the best fit for the second fit as obtained from velocity observations from a sillimanite gneiss of the KTB pilot hole (Berckhemer *et al.*, 1997). Initial and

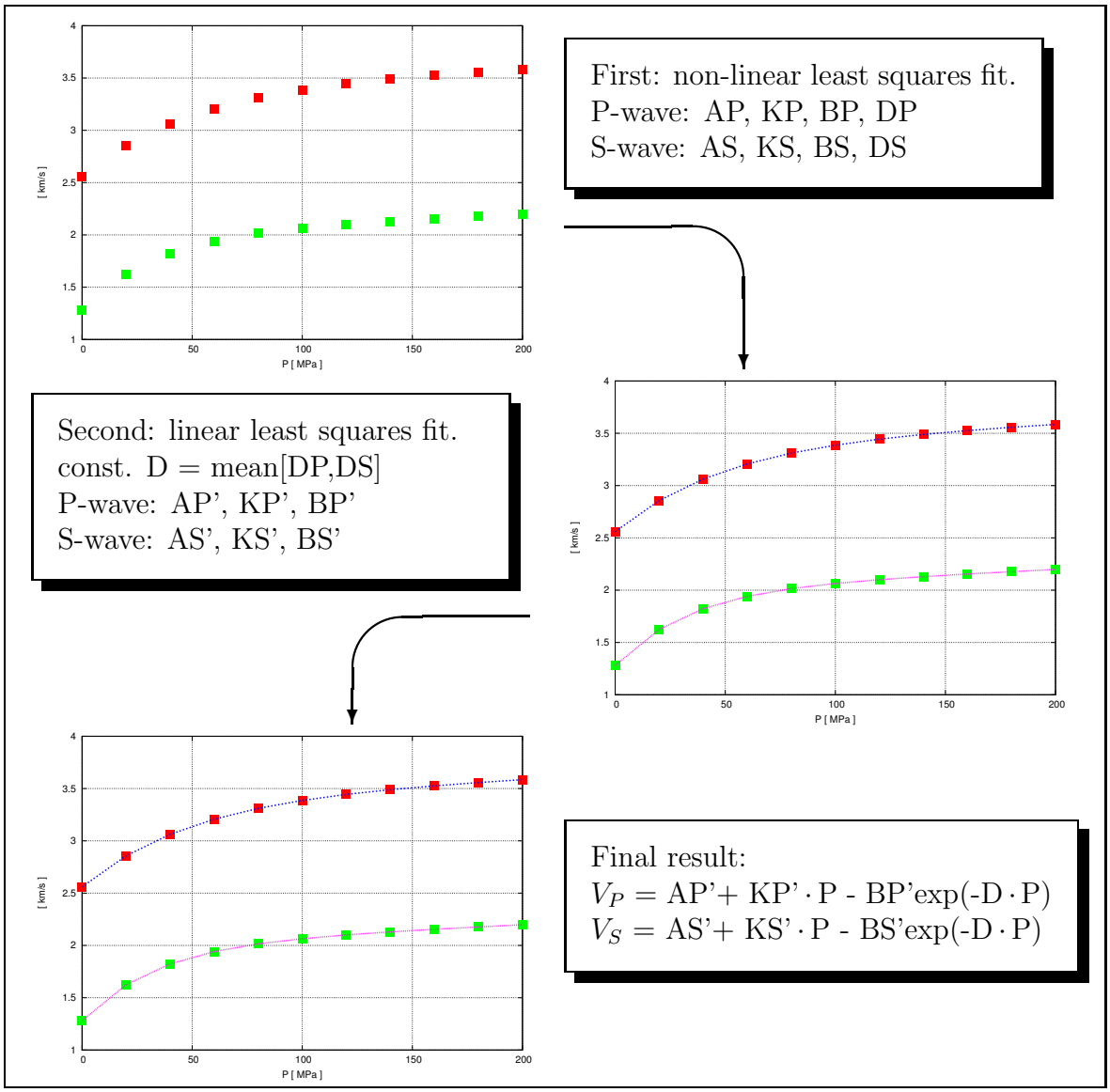

Figure 4.1: Schematic illustration of the two step fit procedure. The fit equation $V = A + K \cdot P - B\exp(-D \cdot P)$ is non-linear in its parameters and their physical meaning depends on the data under consideration. Thus, in the first step, a non-linear least squares fit is separately applied to the all considered data of a certain sample. In a next step the mean of all obtained parameters D is calculated. This D is used as a constant value for all considered data. Taking D as constant value within the second fit procedure makes the fit equation linear in its parameter. Hence, the second fit can be conducted as a standard linear least squares fit.

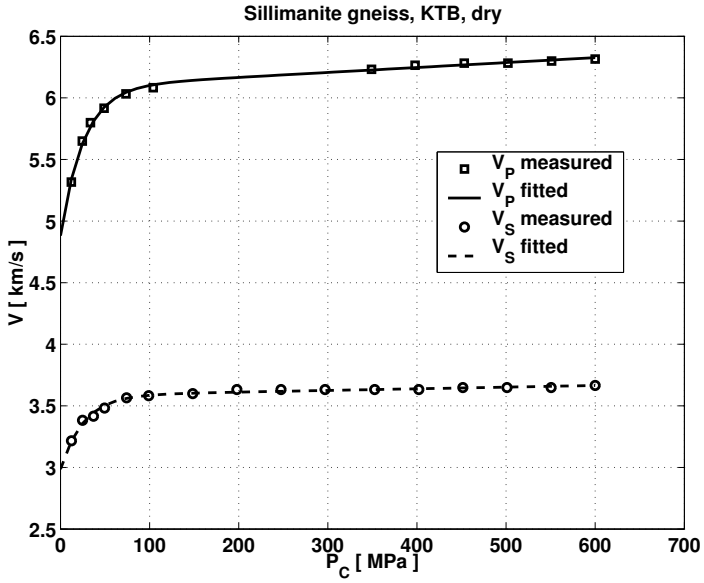

Figure 4.2: Best fit for P-wave (solid line) and S-wave (dashed line) data from a sillimanite gneiss of the KTB pilot hole (Berckhemer *et al.*, 1997). Parameter D was determined to 0.038515 MPa^{-1}.

best fit values are listed in Tab. 4.1. Parameters D_P and D_S agree quite well in the first

Table 4.1: Best fit results for first and second fit. χ^2 gives the sum of the squared deviation of best fit from data. The resulting velocities (for second fit) are plotted with observations in Fig. 4.1

	A_P	K_P	B_P	D_P	χ^2	A_S	K_S	B_S	D_S	χ^2
1. fit	6.052	0.000	1.274	0.045	< 0.001	3.560	0.000	0.556	0.032	< 0.001
2. fit	6.087	0.000	1.205	0.039	0.003	3.585	0.000	0.598	0.039	0.002

fit procedure. Thus, all parameters do not vary remarkably comparing their results for the first and second fit. Although this is an example where the accuracy of the fit slightly decreases from the first to the second fit (compare χ^2 for P- and S-wave fit in Tab. 4.1) the final parameter combination describes the laboratory observations very well as illustrated in Fig. 4.2.

4.2 Elastic properties of isotropic rocks

The changes of elastic moduli of very different rock types as a function of an applied load have been investigated by numerous researchers. Brace (1965) have analyzed the stress dependence of low porosity crystalline rocks and were among the first who identified the dominant role of crack closure on the stress dependence of elastic moduli.

Prasad & Manghnani (1997) focused their studies on the stress dependence of Michigan and Berea sandstone. Differences in the stress dependencies of P-wave velocity and quality factor between both rocks are addressed to distinct microstructures. Pore and confining pressure were varied independently in order to investigate the variation of the effective stress coefficient as a function of both quantities (see eq. 3.3). They found

that pore pressure effects do not cancel confining pressure effects at higher pore and confining pressure. This lead them to the conclusion that the effective stress coefficient is smaller than 1 and a function of pore and confining pressure.

Dvorkin *et al.* (1996) have analyzed the dependence of P- and S-wave velocities of dry sandstones upon effective stress in ultrasonic laboratory experiments. Porosities of the samples varied between 0.05 and 0.3, with a clay content ranging from 0.03 to 0.1. They found that the stress sensitivity of sandstones decreases with increasing porosity and that it was practically independent from clay content.

Eberhart-Phillips *et al.* (1989) have published results of P- and S-wave velocities measurements from 64 different water saturated sandstones as a function of effective stress, porosity, and clay content (C). Effective stress was understood as the difference between confining stress and pore pressure. Since confining stress, and thus effective stress, was isotropic, Eberhart-Phillips *et al.* (1989) use the term effective pressure P_{eff}.

They were able to successfully fit all velocity observations with equation (1.1). The best fit parameters for P- and S-wave velocities as well as the sample names, porosity, and clay content are given in Tab. (1) off their publication. For most samples 17 measurements of P- and S-wave velocities have been conducted and fitted. Samples with less than 6 measurements were ignored. Thus, their data summarize nearly 2000 laboratory measurements. All samples showed an exponential increase in both P- and S-wave velocities up to approx. 20 MPa (0.2kbar) effective stress. Above this stress level the increase in velocities tapers to a flat linear increase (compare Fig. 4.3). They report differences in the stress sensitivity pattern for different rocks, particularly at low effective stress. However, in contrast to Dvorkin *et al.* (1996), they argue that the differences cannot be attributed to porosity.

Eberhart-Phillips *et al.* (1989) found that parameter D was quite similar for the complete data set of 64 P- and corresponding S-wave velocities. A mean D of 0.167±0.053 (for P_{eff} in MPa) was found for all velocities (compare exponential argument in equations (4.4) and (4.5)).

By combining the measurements from all samples, they found empirical best fit equations for P- and S-wave velocity that read:

$$V_p = 5.77 - 6.49\phi - 1.73\sqrt{C} + 0.446\left(P_{eff} - e^{-16.7P_{eff}}\right) \tag{4.4}$$

and

$$V_s = 3.70 - 4.94\phi - 1.57\sqrt{C} + 0.36\left(P_{eff} - e^{-16.7P_{eff}}\right), \tag{4.5}$$

where P_{eff} is in kbar, ϕ and C are dimensionless, and velocities are in km/s. Their model accounts for 95% of the variance and has an rms error of 0.1 km/s. Note, eq. (4.4) and (4.5) were derived from the analyzis of the whole data set. For every single rock sample eq. (1.1) was successfully applied.

Figure 4.3 shows representative P- and S-wave velocities as calculated for best-fit data given by Eberhart-Phillips *et al.* (1989). The porosity of Fontainebleau sandstone (Fig. 4.3(a)) was determined as 0.2 while the clay content was 0.0. In the case of Berea 500 (Fig. 4.3(b)), Conotton (Fig. 4.3(c)), and Coconino sandstone (Fig. 4.3(d)) porosity was 0.195, 0.236, and 0.111 and clay content 0.09, 0.04, and 0.06, respectively.

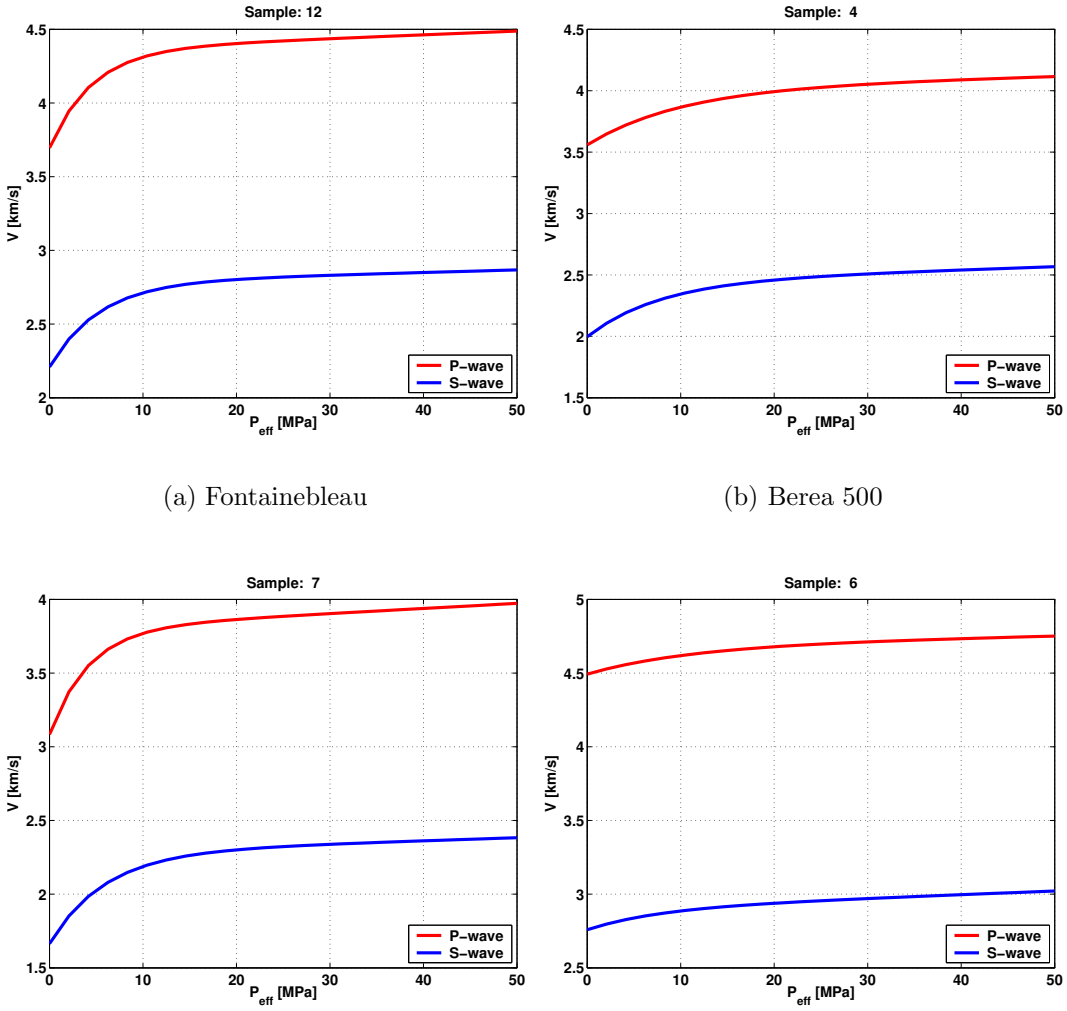

(a) Fontainebleau

(b) Berea 500

(c) Conotton

(d) Coconino

Figure 4.3: P- (red line) and S-wave (blue line) velocities of different sandstones. Velocities were calculated from best fit parameters given in Tab. (1) in Eberhart-Phillips *et al.* (1989).

Unfortunately, only the best fit parameters and porosities of the samples are listed in Eberhart-Phillips *et al.* (1989). As discussed in section (4.1) this corresponds to the first step of the two-step fit procedure, suggested for the application of the stress sensitivity approach. Thus, P- and S-wave velocities for all samples are calculated from the given best fit data. These resulting velocity-stress relations are refitted with parameter $D = (D_P + D_S)/2$ kept constant. Since no observed velocities are given it is not possible to determine the accuracy of the given best fit parameters and the parameters obtained from the refit. The best fit parameters obtained from refitting the velocities are listed in Tab. (F.2). For each sample P- and S-wave velocities could be fitted succesfully with a certain universal parameter D. The parameter K is apprix. zero indicating that stiff pore space closure is negligible for the stress dependence of seismic velocities.

However, Fig. 4.4 shows a comparison of the velocities (shown in Fig.4.3 as lines, here as dots) calculated from the given best-fit parameters with the velocities obtained from refitting. Obviously, the obtained velocities match the given very well.

The same empirical relation (eq. 1.1) was used by Jones (1995) to fit ultrasonic P- and S-wave velocity measurements on different water saturated sandstones at various effective isostatic stresses. The effective stress was defined as the difference between confining stress and pore pressure. Porosity (helium porosity) and density were measured on vacuum-dried samples. Ahead of the velocity measurements the samples were vacuum-saturated with distilled, de-aerated water at a pressure of 10^{-4} Pa.

According to Jones (1995) the parameters K, B, and D do not correlate with porosity or clay content and D is similar for all velocities. In contrast, the pressure independent parameter A shows a linear decrease with initial porosity at room conditions. The physical meaning of parameter A is given in eq. (3.57) and (3.56). It corresponds to the velocity of a rock at $P_{\text{eff}} = 0$ where the porosity consists of the stress independent part ϕ_{s0} of the stiff porosity only. Such an assemblage of spherical inclusions in a homogeneous isotropic material can be described by the upper Hashin-Shtrikman bounds (Hashin & Shtrikman, 1963).

As in the case of the Eberhart-Phillips *et al.* (1989) data set the application of the stress sensitivity approach is impeded by the fact that only the resulting best fit parameters are given and not the velocity observations. Therefore, the velocities for an effective stress up to 60 MPa were calculated for the given best-fit parameters. In the next step the thereby obtained velocities were again fitted, now with a fixed parameter D, calculated as the average of the D values for P- and S-wave given by Jones (1995). Neglecting the stress dependence of density, saturated bulk and shear modulus were calculated and fitted additionally. However, Fig. (4.5) illustrates at least for sample E1(412) that Jones' regression curve matches the observed velocities so well that a refit of the given velocities is still reasonable.

P- and S-wave velocities were calculated for A, K, B, and D. As discussed for the Eberhart-Phillips *et al.* (1989) data set these velocities were refitted. This is illustrated in Fig. (4.6) and the best fit parameters are listed in Tab. 4.2.

Obviously, it was possible to fit the velocities with a very high accuracy. This was expected since the D values given by Jones (1995) are very similar. Thus, the tensor of stress sensitivity of this sample seems to be isotropic.

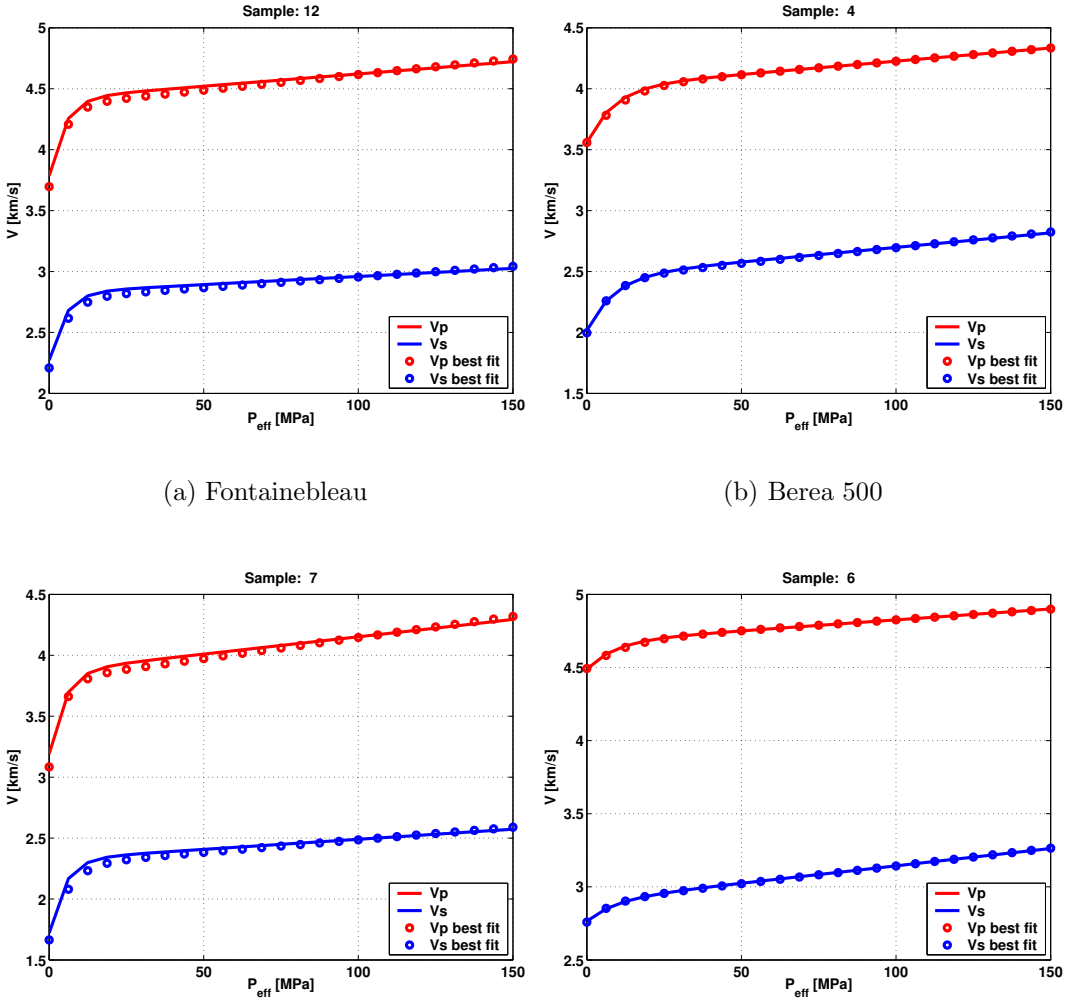

(a) Fontainebleau

(b) Berea 500

(c) Conotton

(d) Coconino

Figure 4.4: P- (red dots) and S-wave (blue dots) velocities calculated from best fit parameters given in tab. (1) in Eberhart-Phillips *et al.* (1989) and velocities calculated from refitted parameters listed in Tab. F.2. Parameter D was 0.205, 0.115, 0.110, and 0.205 (all in 1/MPa) for Fontainebleau, Berea 500, Conotton, and Coconino sandstone, respectively.

Table 4.2: Best fit parameters for regression of velocities for sample E1(412). Fit 1 shows the best fit parameters for this sample given by Jones (1995). Fit 2 gives the best fit parameters obtained from refitting the data with a common and constant parameter D.

	P-wave					S-wave				
	A	K	B	D	χ^2	A	K	B	D	χ^2
Fit 1	4.971	0.001	0.278	0.178	—	3.222	0.001	0.176	0.131	—
Fit 2	4.983	0.001	0.284	0.155	<0.001	3.211	0.001	0.169	0.155	<0.001

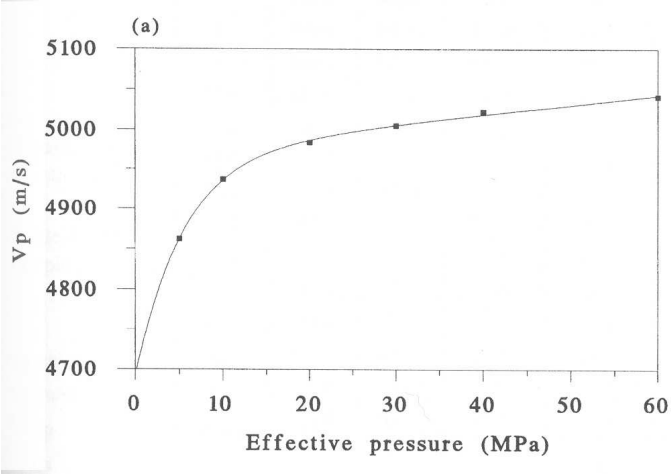

Figure 4.5: This figure was taken from Jones (1995). It illustrates the accuracy of Jones fit results for sample E1(412). Squares denote observed velocities, the line the best fit.

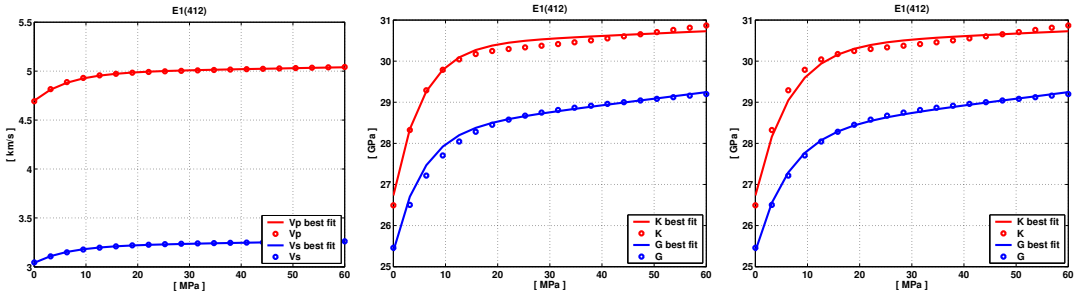

(a) (b) (c)

Figure 4.6: Fig. (4.6(a)): Best fit (solid lines) and velocities (dots) as calculated from Jones (1995). Best fit was done with $D = 0.155 MPa^{-1}$ as the mean of $D_P = 0.178$ and $D_S = 0.131$ given by Jones (1995). Fig. (4.6(b)): Calculated bulk (blue dots) and shear modulus (red dots) and regression (solid lines) where $D = 0.182 MPa^{-1}$ was found. Fig. (4.6(c)): Best fit of moduli with $D = 0.155 MPa^{-1}$ as obtained from velocity regression.

Freund (1992) has published P- and S-wave velocity measurements on 88 clastic rock samples from the Rotliegendes formation. The samples were recovered from well Salzwedel 2/64 in the northern part of Sachsen-Anhalt from 3340 to 3670 m depth. In contrast to Eberhart-Phillips *et al.* (1989) and Jones (1995), he conducted the measurements on oven-dried samples. The samples were dried over 2 weeks at 60° C. All measurements were conducted in a hydrostatic pressure vessel over an effective stress interval ranging from 8 to 300 MPa. Velocities were obtained by pulse-transmission technique whereby ceramic transducers with frequencies of 1MHz were used. The errors in the measurements are given as less than 2% and 3% for P- and S-waves, respectively.

All samples show typical stress dependencies of velocities. In the low pressure regime an increasing load leads to a rapid non-linear increase in both P- and S-wave velocities where P-waves are more sensitive to stress variations than S-waves. For higher stress levels the increase in velocities with increasing stress is linear and shows a very flat slope. The change in P-wave velocity between first loading level (8 MPa) and maximum load (300 MPa) ranges from 6% to 80% for sample 53 and 139, respectively, as shown in Fig. (4.7). The simultaneous increase in S-wave velocity is less pronounced. As for P-wave velocity sample 53 shows the weakest increase of 5% and sample 139 the strongest (53%).

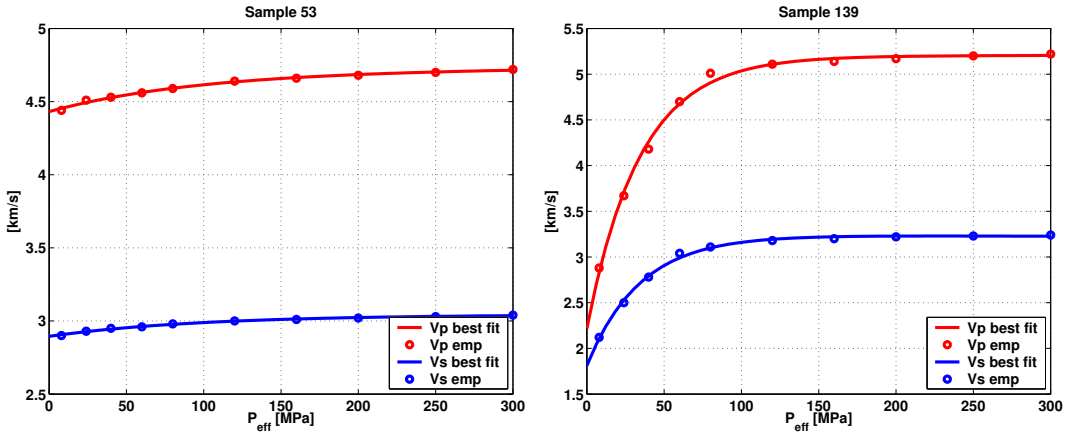

(a) (b)

Figure 4.7: Samples 53 and 139 show the minimum respectively maximum increase in P- and S-wave velocity.

It was possible to fit all 88 P- and S- wave data sets with a high accuracy. The resulting fit parameters for the first and second fit are listed in Tab. (4.3). For some representative samples, a comparison between the measured data and velocities calculated from the the best fit parameters (second fit) listed in Tab. (4.3) is shown in Fig. (4.8).

Obviously, parameter K for both P- and S-wave velocity is approximately zero. Thus, the closure of stiff porosity can be assumed to be negligible over the applied effective stress range. Hence, it is reasonable to assume that the bulk porosity stayed more or less constant during the experiments, since compliant porosity is generally only a very small part of bulk porosity.

Table 4.3: Best fit values for P- and S-wave velocity for example data sets from Freund (1992). Porosity is dimensionless, density in kg/m^3, A in km/s, K in km/s/MPa, B in km/s, D in 1/MPa

Sample	Porosity	Density	Fit	P-wave					S-wave				
				A	K	B	D	χ^2	A	K	B	D	χ^2
120	0.036	2660	1	5.506	0.000	1.920	0.019	0.010	3.555	0.000	0.944	0.023	0.001
			2	5.265	0.001	1.738	0.021	0.003	3.534	0.000	0.924	0.021	0.001
219	0.078	2480	1	4.729	0.000	2.211	0.039	0.009	3.201	0.000	1.253	0.042	0.004
			2	4.745	-0.000	2.134	0.041	0.013	3.233	-0.000	1.211	0.041	0.007
41	0.036	2670	1	4.566	0.000	0.388	0.009	0.001	3.061	0.000	0.265	0.005	0.000
			2	4.685	-0.000	0.505	0.007	0.001	2.970	0.000	0.174	0.007	0.000
95	0.011	2680	1	5.455	0.000	1.009	0.018	0.007	3.149	0.000	0.379	0.019	0.008
			2	5.403	0.000	0.944	0.018	0.006	3.104	0.000	0.313	0.018	0.007
62	0.048	2600	1	4.941	0.000	0.560	0.008	0.003	3.143	0.000	0.328	0.011	0.001
			2	4.835	0.000	0.456	0.009	0.002	3.197	-0.000	0.380	0.009	0.001
53	0.043	2630	1	4.727	0.000	0.297	0.010	0.001	3.041	0.000	0.148	0.011	0.000
			2	4.705	0.000	0.273	0.010	0.001	3.039	0.000	0.144	0.010	0.000
60	0.050	2640	1	4.452	0.000	0.773	0.024	0.011	2.722	0.000	0.381	0.032	0.002
			2	4.426	0.000	0.730	0.028	0.010	2.740	-0.000	0.351	0.028	0.003
56	0.050	2640	1	5.097	0.001	1.504	0.033	0.013	3.503	0.000	0.772	0.019	0.009
			2	5.300	0.001	1.559	0.026	0.023	3.390	0.000	0.666	0.026	0.004
52	0.050	2600	1	4.761	0.000	0.714	0.016	0.001	3.131	0.000	0.398	0.022	0.000
			2	4.631	0.000	0.621	0.019	0.001	3.108	0.000	0.377	0.019	0.000
309	0.086	2450	1	4.859	0.000	2.376	0.036	0.037	3.294	0.000	1.385	0.042	0.005
			2	4.854	0.000	2.265	0.039	0.040	3.350	-0.000	1.312	0.039	0.014
308	0.114	2360	1	4.977	0.000	1.311	0.018	0.004	3.231	0.000	0.815	0.025	0.001
			2	4.847	0.000	1.212	0.021	0.004	3.281	-0.000	0.838	0.021	0.002
294	0.149	2280	1	4.320	0.001	0.940	0.035	0.002	2.927	0.000	0.478	0.032	0.003
			2	4.338	0.001	0.945	0.033	0.002	2.893	0.000	0.434	0.033	0.002
272	0.035	2540	1	5.159	0.001	3.639	0.081	0.008	3.381	0.000	1.225	0.040	0.009
			2	5.271	0.001	3.176	0.061	0.037	3.243	0.001	1.268	0.061	0.003
27	0.018	2680	1	4.799	0.000	0.543	0.016	0.005	3.122	0.000	0.209	0.011	0.000
			2	4.839	-0.000	0.560	0.014	0.006	3.083	0.000	0.172	0.014	0.000

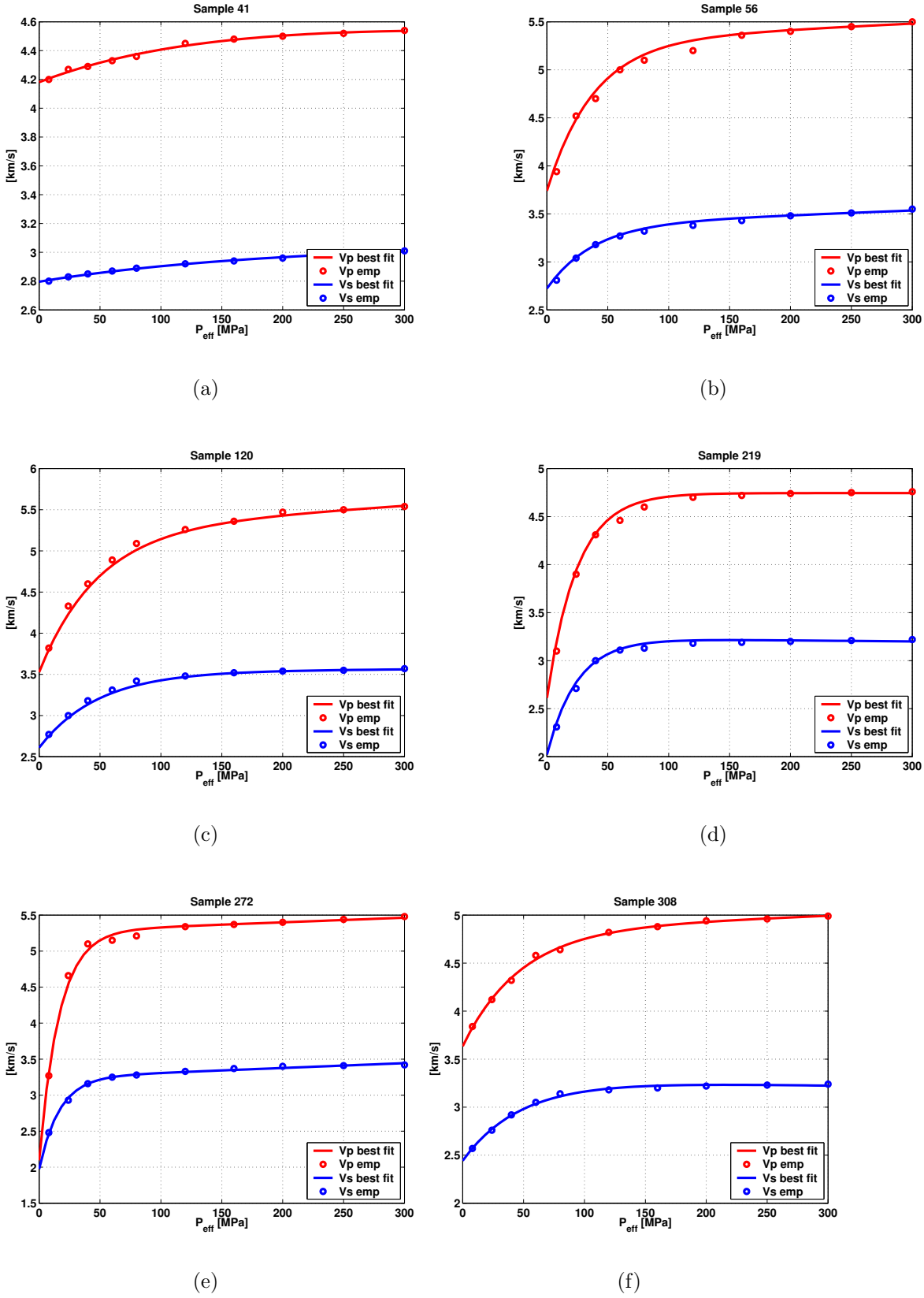

Figure 4.8: Best fit result (solid line) and observations (circles) for P- (red) and S-wave (blue). Velocity data from Freund (1992). Parameter D was 0.007, 0.026, 0.021, 0.041, 0.061, and 0.021 1/MPa in the case of sample 41, 56, 120, 219, 272, and 308, respectively.

If the density of the samples is known it is possible to invert the velocity best fit parameters for the stress sensitivity parameters as described by Shapiro (2003). Although density was determined at room conditions only, it is reasonable that it is approximately constant, since changes in porosity are negligible.

If both P- and S-wave velocities are fitted and the density of the sample is known it is straightforward to invert the fit parameters for the stress sensitivity parameters K_{dryS}, μ_{dryS}, θ_c, $\theta_{c\mu}$, ϕ_{c0} as shown by Shapiro (2003). The results of the inversion for the samples mentioned above are listed in Tab. 4.4 and the results for all samples are listed in Tab. (F.6).

Table 4.4: Stress sensitivity parameters K_{dryS}, μ_{dryS}, θ_c, $\theta_{c\mu}$, $\phi_{\mathrm{c0}}$of sample 41, 56, 120, 219, 272, and 308.

Sample	Porosity [—]	Density [kg/m^3]	K_{dryS} [GPa]	μ_{dryS} [GPa]	θ_c [—]	$\theta_{c\mu}$ [—]	ϕ_{c0} [—]
41	0.036	2670	27.210	23.555	191.747	68.545	0.002
56	0.050	2640	33.717	30.332	887.745	423.865	0.001
120	0.036	2660	29.458	33.214	612.250	369.637	0.001
219	0.078	2480	21.275	25.927	863.338	565.824	0.001
272	0.035	2540	34.953	26.710	2119.854	1013.172	0.001
308	0.114	2360	21.577	25.403	457.892	483.842	0.001

Initial crack porosity was found to be of the order of 0.001, thus it is, indeed, only a very small part of the bulk porosity. θ_c and $\theta_{c\mu}$ are both in the order 10^3, reaching occasionally 10^3. Moreover, θ_c is roughly twice $\theta_{c\mu}$ as shown in Fig. (4.9). Taking all samples into account, this indicates that the dry matrix bulk moduli of the samples are twice as sensitive to changes in compliant porosity than the corresponding matrix shear moduli.

The above mentioned data set confirm that there are rocks where the parameter D is approximately a universal quantity, i.e., that these rocks seem to have an isotropic tensor of stress sensitivity. To illustrate this result Fig. (4.10) shows parameter D_S plotted as a function of corresponding D_P. A linear regression of the data revealed a correlation coefficient of 0.88. The slope of the linear regression was 0.92 with an intercept of 0.003 and a coefficient of determination of R^2=0.78.

According to eq. (3.56) and (3.56) parameter AP and AS represent the stress independent P- and S-wave velocities of the considered rock with closed compliant porosity. This is in agreement with the interpretation of the parameter by Freund (1992). Considering all samples, he found that parameters AP and AS are linear functions of porosity and clay content. Since the density is given for all samples, AP and AS can be used to calculate the corresponding moduli K_{dryS} and μ_{dryS}. This is illustrated in Fig. (4.11). A linear regression was applied to the data. The best fit approximations read:

$$K_{\mathrm{dry}}(\phi) = -151.051 \cdot \phi + 38.4559 \quad (4.6)$$

$$\mu_{\mathrm{dry}}(\phi) = -109.821 \cdot \phi + 32.9837 \quad (4.7)$$

The coefficients of determination R^2 are 0.50 and 0.64 for K_{dry} and μ_{dry}, respectively.

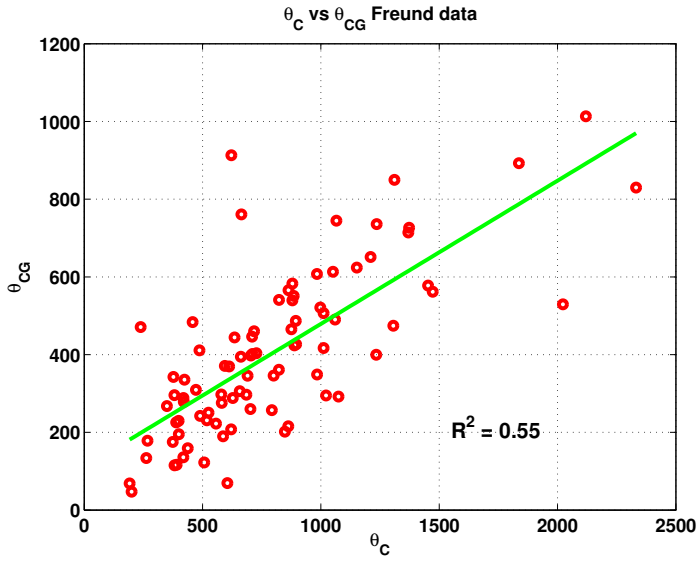

Figure 4.9: Linear regression of θ_c vs. $\theta_c\mu$ for Freund (1992) data set. Least squares fit: y = $0.368\theta_C$ + 110.6, R^2 = 0.55.

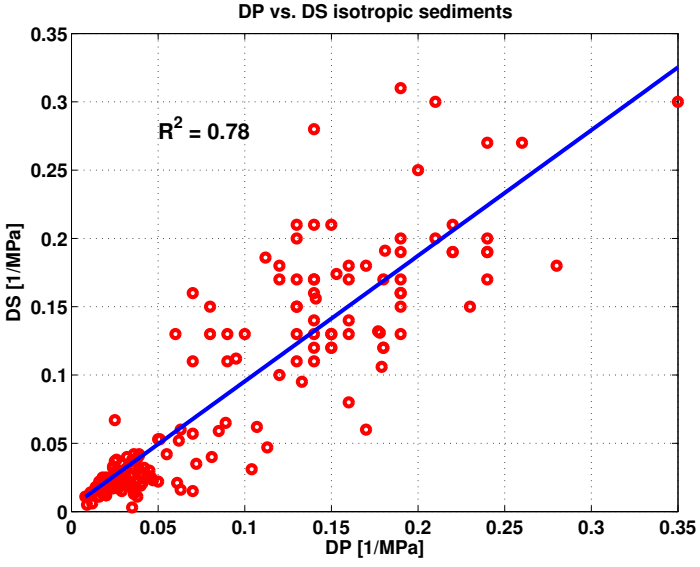

Figure 4.10: Linear regression (blue line) of DP vs. DS (red circles) for all investigated isotropic sandstone samples from Eberhart-Phillips *et al.* (1989); Jones (1995); Freund (1992). Linear regression is y(x)= 0.92x + 0.003 with R^2=0.78.

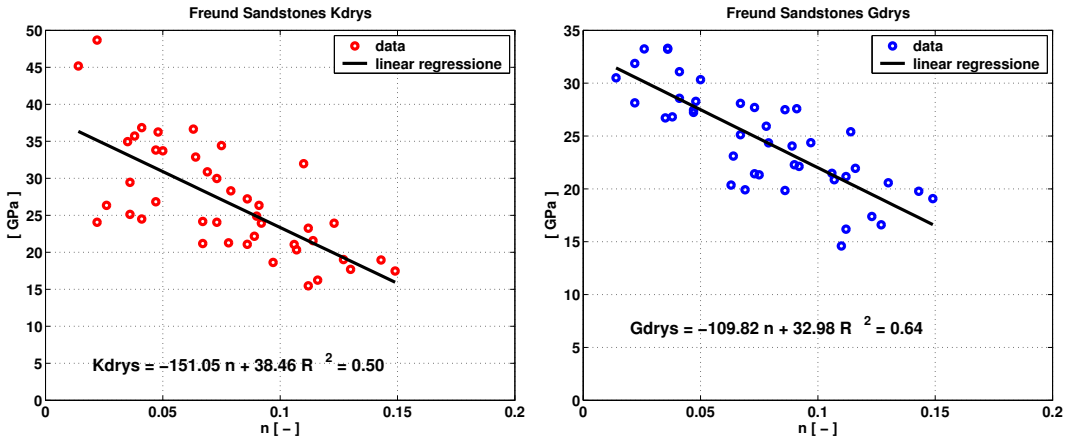

(a) (b)

Figure 4.11: Linear regression of K_{dryS}(Fig. 4.11(a)) and μ_{dryS}(Fig. 4.11(b)) obtained from parameters AP and AS from second fit of Freund (1992) data. Here, porosity is denoted as n.

Beside the pure mathematical linear regression mentioned above, the physical meaning of parameters AP and AS, as derived from the stress sensitivity approach, allow for a physically constrained regression. Since K_{dryS} and μ_{dryS} describe the moduli of a rock with only stiff porosity, i.e., with only spherical inclusions, they should correspond as a function of porosity to the upper Hashin-Shtrikman bounds (Hashin & Shtrikman, 1963).

The Hashin-Shtrikman bounds represent the smallest possible range of effective elastic moduli of a porous medium as a function of the material moduli and porosity. Hence, fitting the upper Hashin-Shtrikman bound to K_{dry} and μ_{dry} over the given porosity range allows for an inversion of the effective bulk and shear modulus K_0 respectively μ_0 of the matrix forming grain material. These grain moduli are need in order to apply Gassmann's equation, e.g., if a fluid substitution analyzis is desired. As shown in Fig. (4.11) K_{dryS} and μ_{dryS} strongly scatter for low porosities. This represents that the complete data set comprises five claystones, 26 siltstones, and 57 sandstone, for which quite different effective grain moduli could be expected. Therefore, it was tried to separate the sandstones from the clay- and siltstones by keeping only those samples with a clay content less than 10%. This might be to restrictive since only 43 and not 57 data samples, as mentioned by Freund (1992), remained. However, the resulting best fit of the upper Hashin-Shtrikman bounds to K_{dryS} and μ_{dryS} are shown in Fig. (4.12).

While the approximation of μ_{dryS} was quite successful, it is obviously less convenient for K_{dryS}. Using the upper Hashin-Shtrikman bound as an envelope was even worse. If the derived physical meaning of parameter A is reasonable this indicates that the mineralogical composition of the sandstones is probably not uniformly enough to be represented with one effective mineral phase.

However, this example illustrates the advantage of using a physically constrained regression based on the stress sensitivity approach instead of a pure mathematical analyzis. It allows to decide physically constrained if the regression is sufficient for a

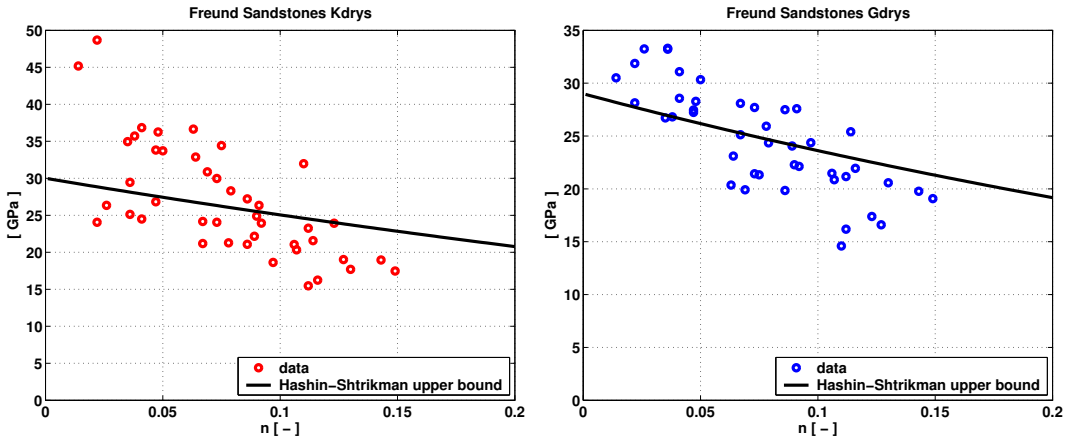

(a) (b)

Figure 4.12: Regression of K_{dryS} (Fig. 4.12(a)) and μ_{dryS} (Fig. 4.12(b)) from sandstones with the upper Hashin-Shtrikman bound. Bulk and shear modulus K_0 and μ_0 of effective grain material are 30 and 29 GPa, respectively.

certain task.

4.3 Elastic properties of anisotropic rocks

Lo *et al.* (1986) investigated the elastic properties of vacuum dried Berea sandstone, Chicopee shale and Chelmsford granite at confining isostatic stress up to 100 MPa using ultrasonic transmission method. All samples were treated as transversely isotropic. Therefore, P-wave velocity was measured in the 1 (V11) and three direction (V33) together with the corresponding S-wave velocities VSH1, VSV1, VSH3a, and VS3b. In addition, VP and VSH as well as VSV were observed at an angle of 45° with respect to the 3 axis. In the case of the sedimentary rocks Berea sandstone and Chicopee shale the 3 axis was oriented normal to the bedding plane which was assumed to represent the plane of isotropy. For Chelmsford granite the plane parallel to the cracks, denoted as the "fit plane", was defined as the plane of isotropy. Three cylindric samples were cut for each rock with respect to the assumed plane of isotropy.

A total of nine velocities was measured for each sample and six were used to calculate the five independent entries of the stiffness matrix. VSH3a and VSH3b were averaged to determine C_{44}. Using an index notation for the velocities V_{ij} where i denotes the direction of propagation and j the polarization direction we obtain: VSH1 → V12, VSV1→ V13, VSH3a/b → V31, VP11 → V11, and VP33 → V33. From observations in the 45° direction only P-wave velocity was used, hence VP45 → V45.

The porosity of Berea sandstone was 17%. P-wave velocities increase by 21% from approx. 3.2 to 4.1 km/s while S-wave velocity increases from 2.1 to 2.7 km/s (Fig. 4.13(a)) by 22%. In general, anisotropy is weak and becomes less with increasing load indicating the influence of crack closure on anisotropy, clearly shown by Thomsen's anisotropy parameters (Fig. 4.13(c)). The stiffnesses C_{12}, C_{13}, C_{44}, and C_{66} are

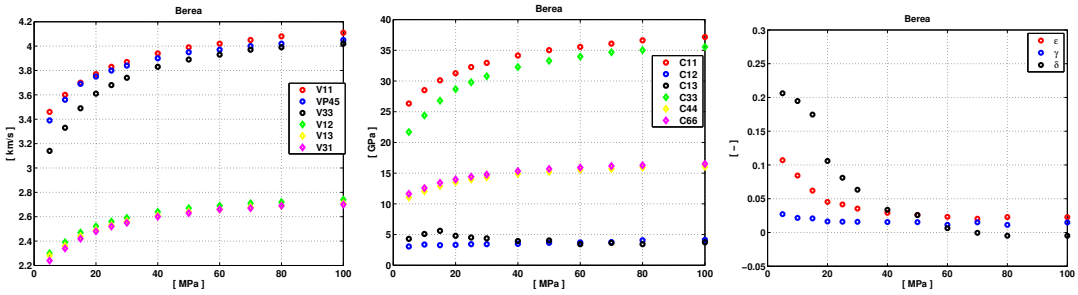

(a) (b) (c)

Figure 4.13: Velocities (Fig. 4.13(a)), stiffnesses (Fig. 4.13(b)), and Thomsen parameters (Fig. 4.13(a)) of Berea sandstone. Velocities from Lo *et al.* (1986)

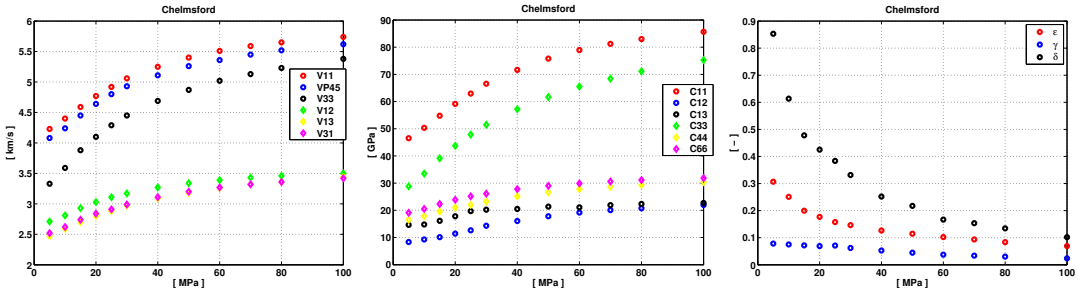

(a) (b) (c)

Figure 4.14: Velocities (Fig. 4.14(a)), stiffnesses (Fig. 4.14(b)), and Thomsen parameters (Fig. 4.14(a)) of Chelmsford granite. Velocities from Lo *et al.* (1986)

less sensitive to stress than C_{11}, and C_{33}

The porosity of Chelmsford granite was 0.9%. P-wave velocities increase by approximately 36% from around 3.5 to 5.5 km/s (Fig. 4.14(a)). S-wave velocities increase by 29% from roughly 2.5 to 3.5 km/s. Thus, especially P-wave velocity is more sensitive to stress increase than in the case of Berea sandstone. Elastic anisotropy is strong up to 50 to 60 MPa and depends remarkably on stress as shown by the Thomsen's parameters (Fig. 4.14(b)). This indicates that the anisotropy is mainly caused cracks.

In contrast, the anisotropy of Chicopee shale is mainly controlled by the bedding plane and minor contributions of mineral constituents. S-wave velocities are more or less independent from stress. P-wave velocities increase by 10% and less (Fig. 4.15(a)). The anisotropy of Chicopee shale is weak. Especially Thomsen's parameter δ is small and fluctuates around zero (Fig. 4.15(c)). Parameter ϵ decreases continously while γ stays more or less constant.

The stress dependence of anisotropy of the samples was investigated in terms of stress sensitivity. For every sample every velocity was separately fitted. The obtained D values were averaged and all velocities were refitted with this single parameter D. Figure 4.16 compares the observed velocities with the best fit results. The best fit

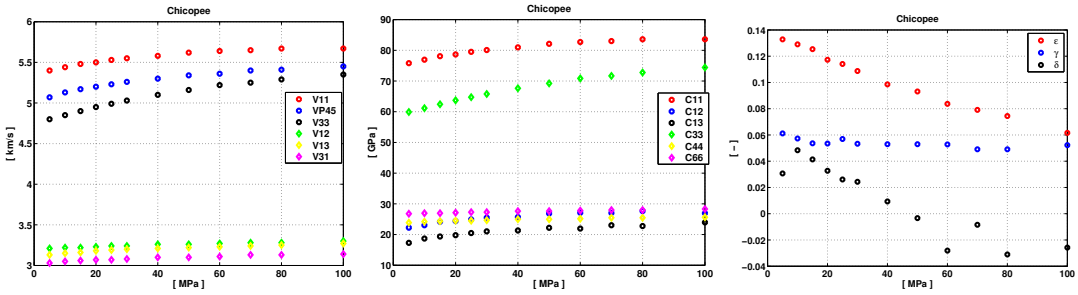

(a) (b) (c)

Figure 4.15: Velocities (Fig. 4.15(a)), stiffnesses (Fig. 4.15(b)), and Thomsen parameters (Fig. 4.15(a)) of Chicopee shale. Velocities from Lo *et al.* (1986)

parameters are listed in Tab. (4.5).

All velocities of all samples could be fitted with a very high accuracy in both the fist and second fit step. The closure of stiff porosity is negligible for all samples, since parameter K is approximately zero. Comparing the best for parameters of both steps shows that they vary only slightly. This is due to the similarity of parameter D for all velocities in the first fit step, especially in the case of Berea sandstone. This indicates that the tensor of stress sensitivity of all three samples is isotropic.

Since the samples were isostatically loaded an isotropic tensor of stress sensitivity should result in a stress independent elastic anisotropy, hence, in constant Thomsen's parameters. However, only parameter γ seems to correspond to this theoretical condition. Berea sandstone and Chelmsford granite show an approximately constant parameter ϵ above 20 MPa load while it continously decreases for Chicopee shale. The strongest sensitivity to stress is shown by parameter δ below 40 MPa load, especially in the case of Chelmsford granite.

There are a couple of possible reasons for this discrepancy between the theoretically required stress independence of anisotropy and observations which might even occur in combination. In the case of Berea sandstone and Chicopee shale the anisotropy is small even in the low stress regime. Especially Berea sandstone approaches elastic isotropy above 40 MPa. Thus, measurement errors occurring especially in the low stress regime might effect anisotropy. However, it is most likely that the orientation of the measurement coordinate system with respect to the rock texture might produced a tilt of the true from the assumed TI symmetry axis. Moreover, it is also possible that the rocks are only apparently transversely but, in fact, slightly orthorhombicaly isotropic. In this case, a misalignment of the measurement coordinate system from the symmetry planes might also result in the observed behavior of Thomsen's parameters.

4.4 Anisotropic metamorphic rocks from the KTB

The following part shows results from the application of the stress sensitivity approach to velocity vs. isostatic stress data from anisotropic metamorphic rock samples from the

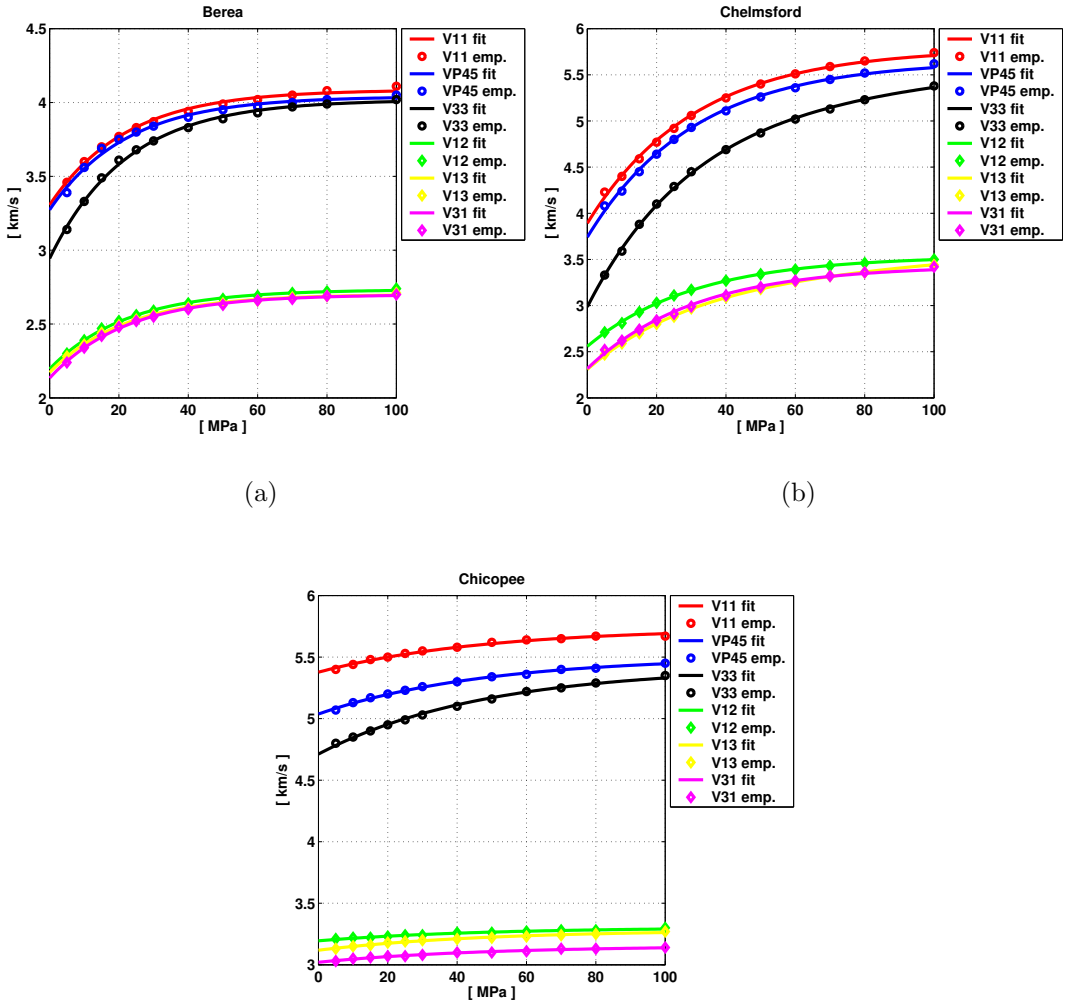

(a) (b)

(c)

Figure 4.16: Measured velocities and best fits for Berea sandstone (Fig. 4.16(a)), Chelmsford granite (Fig. 4.16(b)), and Chicopee shale (Fig. 4.16(c)). Parameter D was 0.045, 0.032, and 0.021 per MPa, respectively. Velocities from Lo *et al.* (1986)

Table 4.5: Best fit results for first and second fit of velocity data from Lo *et al.* (1986).

Sample	Fit	Velocity	A [km/s]	K [km/s/MPa]	B [km/s]	D [1/MPa]	χ^2
Berea sandstone	1	V11	4.105	0.000	0.766	0.040	0.002
		VP45	4.026	0.000	0.788	0.050	0.004
		V33	4.008	0.000	1.086	0.048	0.002
		V12	2.735	0.000	0.534	0.044	0.000
		V13	2.707	0.000	0.525	0.043	0.000
		V31	2.698	0.000	0.567	0.046	0.001
	2	V11	4.086	0.000	0.780	0.045	0.002
		VP45	4.041	0.000	0.768	0.045	0.005
		V33	4.018	0.000	1.074	0.045	0.002
		V12	2.733	0.000	0.537	0.045	0.000
		V13	2.702	0.000	0.530	0.045	0.000
		V31	2.699	0.000	0.565	0.045	0.001
Chelmsford granite	1	V11	5.852	0.000	1.901	0.028	0.002
		VP45	5.716	0.000	1.919	0.029	0.004
		V33	4.822	0.006	1.890	0.041	0.002
		V12	3.531	0.000	0.979	0.033	0.001
		V13	3.160	0.003	0.859	0.036	0.001
		V31	3.499	0.000	1.128	0.026	0.000
	2	V11	5.784	0.000	1.893	0.032	0.006
		VP45	5.654	0.000	1.913	0.032	0.007
		V33	5.199	0.003	2.213	0.032	0.003
		V12	3.537	0.000	0.979	0.032	0.001
		V13	3.260	0.002	0.952	0.032	0.000
		V31	3.433	0.000	1.115	0.032	0.004
Chicopee shale	1	V11	5.697	0.000	0.342	0.029	0.000
		VP45	5.490	0.000	0.458	0.023	0.000
		V33	5.498	0.000	0.761	0.016	0.000
		V12	3.317	0.000	0.117	0.016	0.000
		V13	3.276	0.000	0.161	0.023	0.000
		V31	3.159	0.000	0.137	0.019	0.000
	2	V11	5.735	0.000	0.357	0.021	0.001
		VP45	5.503	0.000	0.466	0.021	0.000
		V33	5.417	0.000	0.705	0.021	0.001
		V12	3.304	0.000	0.109	0.021	0.000
		V13	3.282	0.000	0.164	0.021	0.000
		V31	3.154	0.000	0.134	0.021	0.000

pilot hole of the German Continental Deep Drilling Program (KTB). The measurements were conducted at the Mineralogical-Petrographical Institute, University Kiel. Here, a short summary of the experimental set up is given in so far, as it is important for the application of the stress sensitivity approach. A detailed description can be found in Kern & Schmidt (1990); Kern *et al.* (1991, 1994).

One key issue of the laboratory experiments was the determination of physical in situ properties of the KTB rocks. Petrophysical rock characteristics like elastic wave velocity, velocity anisotropy, shear wave splitting, density, crack porosity and radiogenic heat production were measured over an effective stress and temperature range up to 600 MPa and 600° C, respectively.

For the velocity determination 2 MHz transducers are fixed to the back end side of the pistons. Ultrasonic piezo elements alow for the determination of one P- and two orthogonally polarized S-waves in each piston direction. The S-wave receivers are oriented parallel to the cube edges. Therefore, the travel time through the sample is obtained by subtracting the calibrated time needed for the pulse to travel to and from the sample through the pistons from the total time measured by the transducers. This technique allows for the simultaneous determination of three P- and six- corresponding S-wave velocities as well as a direct observation of sample length changes in the three orthogonal directions with increasing stress and temperature. The error for the determination of the seismic velocities is given as less than 1-2% for confining stresses larger than 200 MPa (Popp, 1994). In addition, the deformation of the samples in the three coordinate directions due to the applied load was measured. However, Popp (1994) gives errors up to 10% for the strain measurements.

The samples used here cover a depth interval between 1546.85 m and 3885.69 m. The experiments were carried out on cubic dry samples with 43 mm initial edge length in a cubic anvil apparatus using the pulse transition technique (for details see Kern, 1982). Six pyramidal pistons are pressed in three orthogonal directions on the cubic sample to apply a near-isostatic stress. The edges of the samples are with 1 to 2 mm slightly larger than the contact sides of the pistons to account for the volume reduction due to compression. The resulting free edges are sloped to guarantee a homogenous stress distribution through out the sample.

The samples were oriented in the apparatus with respect to the macroscopically visible texture, i.e., foliation and lineation. The x- and y-axis are oriented in the plane of foliation, the z-axis normal to it. The x-axis is aligned parallel to lineation, the y-axis orthogonally (Kern *et al.*, 1991). The deviation of opposite sides of the cubic samples from parallelism was 1/100 mm (Popp, 1994). To minimize friction between the sample sides and the pistons the samples were sprayed with graphite.

All KTB data used here were measured on dry samples. The usage of dry samples in ultrasonic velocity measurements has the advantage that frequency dependent Biot type effects do not have to be taken into account. The stress dependent velocities of ten randomly chosen samples were analyzed (Tab. 4.6).

The rocks are assumed to show either an orthorhombic or a more or less transversel isotropy (Kern *et al.*, 1991). However, the laboratory experiments were not conducted in order to describe in detail the stress dependence of seismic velocities and anisotropy. The main focus was on more general investigations of the stress dependence of various

Name	d [m]	P [MPa]	ϕ_c [%]	Rock type
514 KTB 324 E11	1546.85	43.31	0.619	Meta-Gabbro
403 Cli 515	1783.03	49.92	0.004	Sillimanite-Muscovite-Biotit-Gneiss
602 A2a (530)	2471.10	69.19	0.351	Granat-Sillimanit-Biotit-Gneis
522 KTB 607 Albk	2485.75	69.60	0.392	Granat-Hornblende-Biotit-Gneiss
692 F1s (545)	2839.47	79.50	0.491	Sillimanit-Biotit-Gneis
KTB 737 B1d (549)	3011.44	84.32	0.194	Granat-Sillimanit-Muskovit-Biotit-Gneis
742 A1a (554)	3031.00	84.87	0.331	Lamprophyr
KTB 872 F1n (555)	3560.00	99.70	0.360	Sillimanite-Muscovite-Biotit-Gneiss
KTB 919 E1k (568)	3762.97	105.36	0.335	Granat-Amphibolit
KTB 955 C1e (558)	3885.69	108.80	0.560	Biotit-Hoernblende-Gneiss

Table 4.6: Name, depth (d), in situ pressure (P), surface crack porosity ϕ_c, and rock type of the samples.

rock physical properties. Therefore, the cubic samples were cut with respect to the macroscopically visible fabric elements, i.e., the foliation and, if present, lineations. Assuming transversally or orthorhombically isotropic media it is reasonable to identify the foliation as a significant reason for seismic anisotropy and, hence, in a first approximation, the foliation plane as a plane of symmetry (orthorhombic medium) or even the plane of isotropy (TI medium). However, this is just a rough approximation since (a) the alignment of the phyllosillcates is probably not perfectly parallel and a possible additional anisotropy due to (a) a preferred orientation of other anisotropic minerals as well as (c) cracks is neglected. As a result it is possible that the foliation plane is tilted with respect to the seismically effective symmetry (isotropy) plane. However, assuming that the foliation plane represents a symmetry or isotropy plane in an orthorhombically or transversely isotropic medium, respectively, the direction of the measurement coordinate system normal to the foliation plane is denoted as the 3-direction.

Both remaining directions lie within the foliation plane. They are distinguished with respect to the orientation of the lineation. Per definition, the 1-direction is oriented parallel and the 2-direction orthogonal to the lineation. In a TI medium this definition is arbitrary since the foliation plane should represent the plane of isotropy. However, in a rectangular measurement coordinate system with one axis parallel to the symmetry axis only four independent velocities can be measured. Hence, the inversion of the complete TI stiffness tensor is impossible.

If the medium is orthorhombic this definition of the reference coordinate system is insufficient for the determination of the orthorhombic stiffness tensor. The nine independent entries can be inverted from the velocity measurements only if they are conducted in the planes of symmetry. Thus, it is most probable that the 1- and 2-direction of the measurement coordinate system do not coincide with the symmetry planes as illustrated in Fig. 4.17.

Figure (4.18) shows representative velocity-stress and strain-stress data of the KTB samples 403Cli515 and KTB955C1e558. In the case of sample 403Cli515 three distinct P-wave velocities were observed (Fig. 4.18(a)). The P-wave velocity in the three direction, normal to the macroscopically visible plane of foliation, is the slowest, approximately 1 km/s slower than V22 and V33 below 300 MPa effective stress. Above

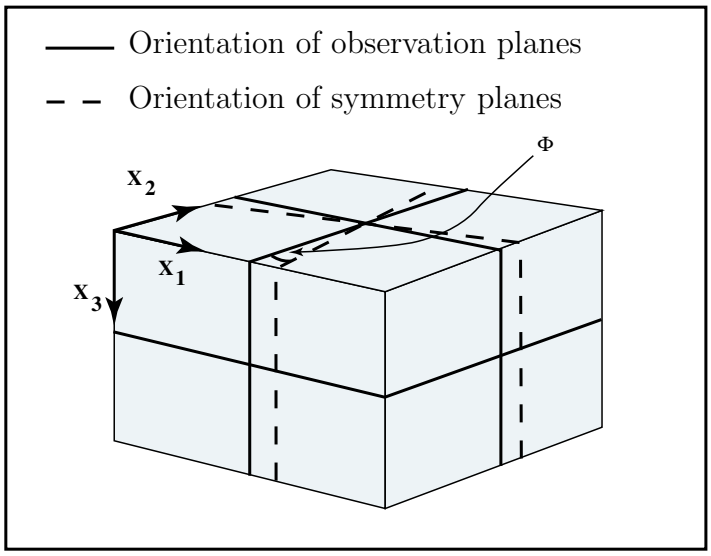

Figure 4.17: Mismatch between the measurement coordinate system and the symmetry planes of orthorhombic medium.

400 MPa V33 increases stronger than V11 and V22. This corresponds to the behavior of the simultaneously observed strains. Although S-waves do not show this post-400 MPa increase this could indicate that for higher stress the stiff porosity closure becomes non-linear and/or the grain stiffness becomes stress dependent, hence, the stress sensitivity approach is no longer valid.

The mean strain reaches approx. 0.4% at 300 to 350 MPa. In contrast, the P- and S- velocities change over the same range of applied stress with respect to the velocities at 25 MPa by 3-7 and 2-8%, respectively. If we assume that the bulk deformation of the sample below 350-400 MPa is a measure of the deformation of the pore space only, this shows, that the influences of stress on velocities is one orders of magnitude larger than on bulk porosity. However, in the case of sample KTB955C1e558 velocities increase by 20-30% while strain reaches approx. 0.4%, hence the stress sensitivity of velocities is 2 orders of magnitude larger.

Both stress-strain relations in 1 and 2 direction of sample KTB955C1e558 (Fig. 4.18(f)) clearly show a bulge below 350 MPa. Since there is no corresponding effect observable in the velocities this might illustrate the higher strain measurement errors with respect to velocity error.

Due to the above mentioned indications for a limited validity of the stress sensitivity approach for higher stresses, the following considerations are restricted to observations below 350 MPa inclusively.

Figure (4.19) shows the comparison between the observed velocities and the best fit, sorted according to the direction of propagation. As mentioned above only V33 shows a remarkable stress sensitivity while the remaining velocities change only slightly with stress. In summary, all velocities become approximately independent from stress above 150 MPa. This might indicate the crack closing stress for sample 403Cli515 and that the closure of stiff porosity seems to be negligible. According to T. Popp (pers. communication) core observations indicate that the KTB rocks show no stiff porosity at all.

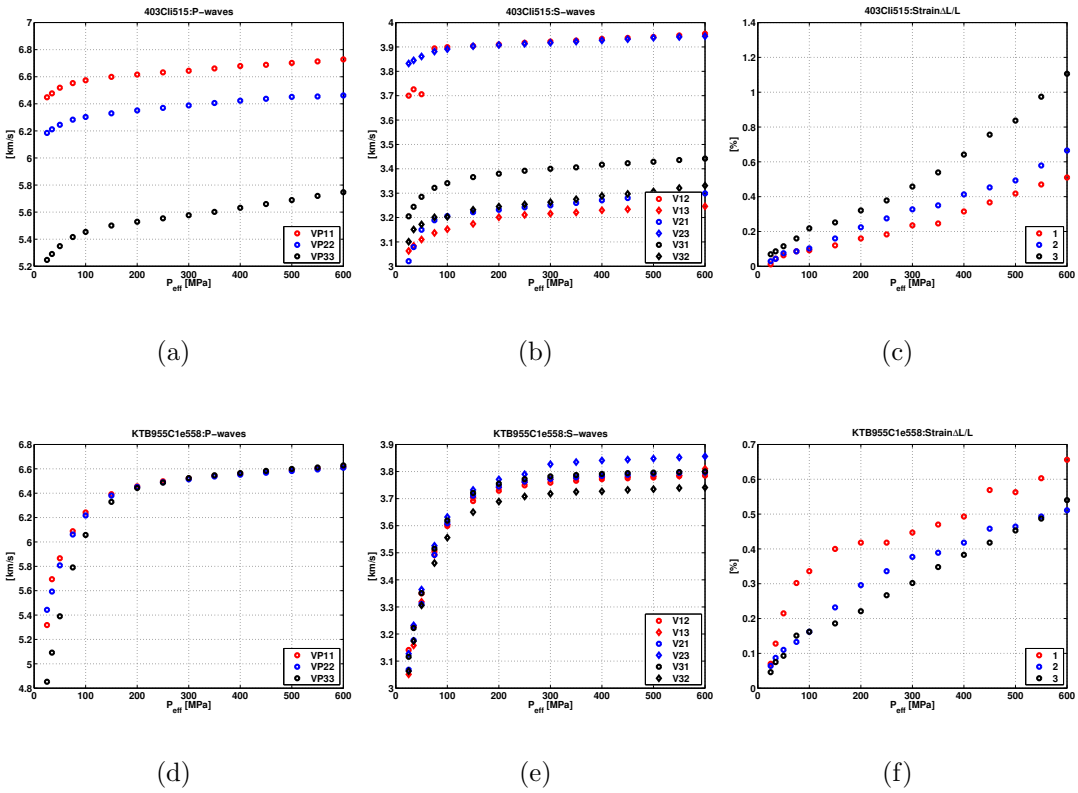

Figure 4.18: Velocities and strain for sample 403Cli515 (4.18(a) - 4.18(c)) and KTB955C1e558 (4.18(d) - 4.18(f)).

The interpretation of a negligible role of stiff porosity closure for the stress sensitivity of the sample is supported by the best fit parameters, listed in tab. 4.7. For all velocities parameter K is smaller than 0.001.

Sample KTB955C1e558 (see Fig. 4.18 and 4.20) shows a remarkable stronger increase in seismic velocities with stress than sample 403Cli515. The velocities approach a constant level at 200 MPa effective stress, indicating a slightly higher crack closing stress than found for sample 403Cli515. A comparison of the three P- and the six S-wave velocities shows that the sample is approximately isotropic, especially above 200 MPa. This is a hint that the weak anisotropy of the sample below 200 MPa is crack induced. The difference in the stress dependence of velocities and anisotropy was unexpected since both rocks are gneisses.

Figure (4.21) comprises the best fit D parameters for all P- and S-wave data. For every direction the two D values of the S-waves are plotted against the corresponding DP value. The data scatter around the solid line indicating DP = DS with a correlation coefficient of 0.59. The linear regression of the data gave $DS = 0.503DP + 0.01$ with a coefficient of determination of $R^2 = 0.35$.

Although a detailed analyzis of the stress dependent anisotropy was not possible due to uncertainties about the orientation of the measurement coordinate system with respect to the orthorhombic symmetry planes, it was possible to calculate at least Tsvankin's parameters ϵ and γ. Fig. (4.22) shows the anisotropy parameters for weak anisotropic samples. In all cases, the anisotropy is approximately independent from

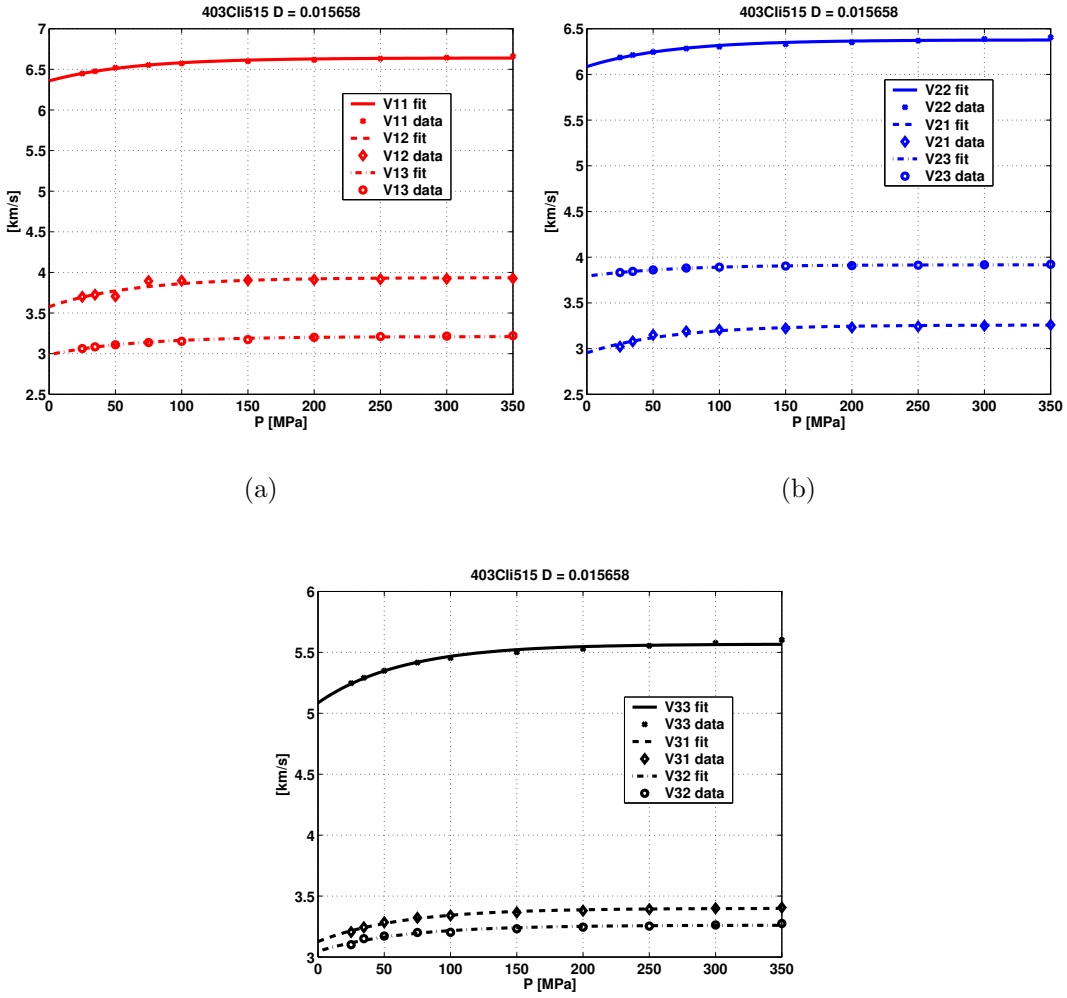

(a) (b)

(c)

Figure 4.19: Velocities and best fit for KTB sample 403Cli515. Fig. 4.19(a) shows velocities in 1, Fig. 4.19(b) in 2, and Fig. 4.19(c) in 3 direction. A universal parameter D = 0.016 per MPa was found.

Table 4.7: Best fit parameters for KTB sample 403Cli515. Velocities are in km/s, A is in [km/s], K in [km/s/MPa], and D in [1/MPa]. χ^2 is dimensionless.

	First fit					Second fit				
Vel.	A	K	B	D	χ^2	A	K	B	D	χ^2
V11	6.651	0.000	0.262	0.012	0.001	6.640	0.000	0.282	0.016	0.001
V12	3.924	0.000	0.429	0.022	0.010	3.937	0.000	0.358	0.016	0.011
V13	3.225	0.000	0.203	0.010	0.000	3.211	0.000	0.224	0.016	0.001
V22	6.404	0.000	0.263	0.009	0.001	6.378	0.000	0.292	0.016	0.002
V21	3.242	0.000	0.445	0.029	0.001	3.258	0.000	0.304	0.016	0.003
V23	3.917	0.000	0.124	0.016	0.000	3.917	0.000	0.125	0.016	0.000
V33	5.590	0.000	0.443	0.011	0.001	5.568	0.000	0.483	0.016	0.002
V31	3.398	0.000	0.278	0.017	0.000	3.400	0.000	0.273	0.016	0.000
V32	3.263	0.000	0.210	0.015	0.001	3.261	0.000	0.214	0.016	0.001

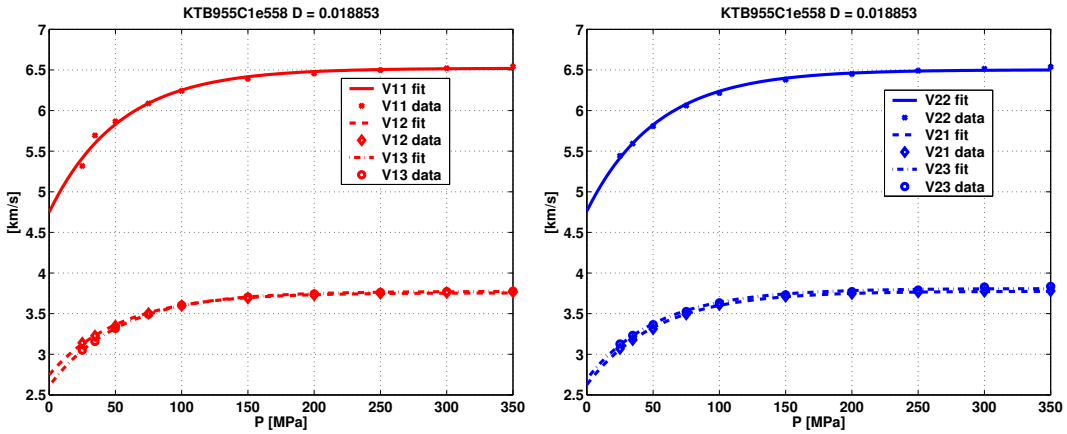

(a)

(b)

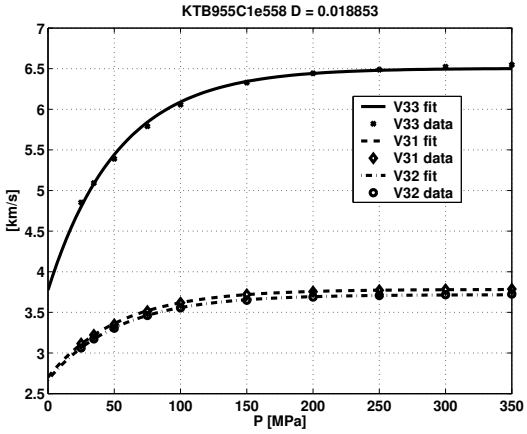

(c)

Figure 4.20: Velocities and best fit for KTB sample 955C1e558. Fig. 4.20(a) shows velocities in 1, Fig. 4.20(b) in 2, and Fig. 4.20(c) in 3 direction. A universal parameter D = 0.019 per MPa was found.

Table 4.8: Best fit parameters for KTB sample KTB955C1e558. For units see Tab. (4.7)

	First fit					Second fit				
Vel.	A	K	B	D	χ^2	A	K	B	D	χ^2
V11	6.287	0.001	1.947	0.029	0.013	6.521	0.000	1.772	0.019	0.022
V12	3.764	0.000	0.968	0.017	0.000	3.756	0.000	1.008	0.019	0.001
V13	3.773	0.000	1.168	0.019	0.000	3.774	0.000	1.167	0.019	0.000
V22	6.524	0.000	1.640	0.017	0.001	6.502	0.000	1.739	0.019	0.004
V21	3.779	0.000	1.132	0.018	0.000	3.776	0.000	1.150	0.019	0.001
V23	3.823	0.000	1.053	0.017	0.001	3.809	0.000	1.114	0.019	0.002
V33	6.546	0.000	2.551	0.016	0.001	6.504	0.000	2.729	0.019	0.012
V31	3.787	0.000	1.058	0.018	0.000	3.783	0.000	1.080	0.019	0.000
V32	3.721	0.000	1.034	0.018	0.000	3.718	0.000	1.050	0.019	0.000

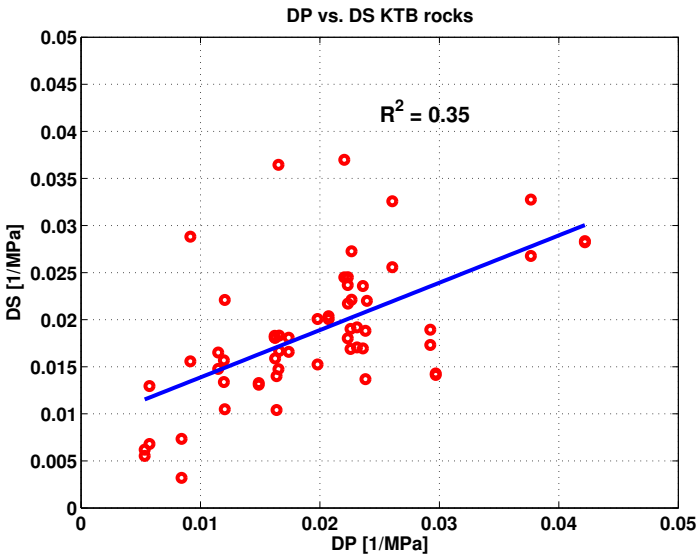

Figure 4.21: DP vs. DS plot for all velocities of the KTB data set. Solid line indicates DP=DS. Linear regression: DS = 0.503DP + 0.01, $R^2 = 0.35$.

stress. In the case of isostatic effective stress, a stress independent anisotropy indicates a tensor of stress sensitivity with only one effectively independent element, as can be found in the case of isotropic rocks. This corresponds quite well the result of the velocity fits, where all velocities of a certain sample could be fitted successfully with a constant parameter D. Variations occur only at low stress. Only in the case of sample 955C1e558 (Fig. 4.22(b)) the ϵ parameters strongly vary.

Sample 403Cli515 and 692F1s545 illustrated in Fig. (4.23) show a stronger anisotropy (above 10%). The anisotropy seems to depend on the applied load and decreases with increasing stress. The decrease of anisotropy is in contrast to the universality of parameter D found from the velocity fits. However, this discrepancy might indicate that the tensor of stress sensitivity of both samples has more than one effectively independent entry. However, it might also result from the limitation of the stress dependent Tsvankin's parameters to weak anisotropic media, since the anisotropy of both samples is not weak.

4.5 Stress dependent electrical resistivity.

Brace *et al.* (1965) have published data from stress dependent deformation and electrical resistivity measurements simultaneously conducted on low porosity crystalline rocks. The samples were isostatically loaded up to 1 GPa (10 kbar), whereby a constant pore fluid pressure of approx. $P_{fl} = 0$ was maintained during the experiments. Although all measurements were conducted on saturated samples the pore pressure during compression was maintained approx. zero. Tap water, with a resistivity $\Omega_t = 45 - 50 ohmm$ and a NaCl solution ($\Omega_s = 0.3 ohmm$) were used as saturating fluids. The suite of samples generally shows bulk porosities below 1%. In this study, we used five rocks, namely Casco, Stone Mountain, and Westerly granite as well as Rutland quartzite, and Cape Cod granodiorite.

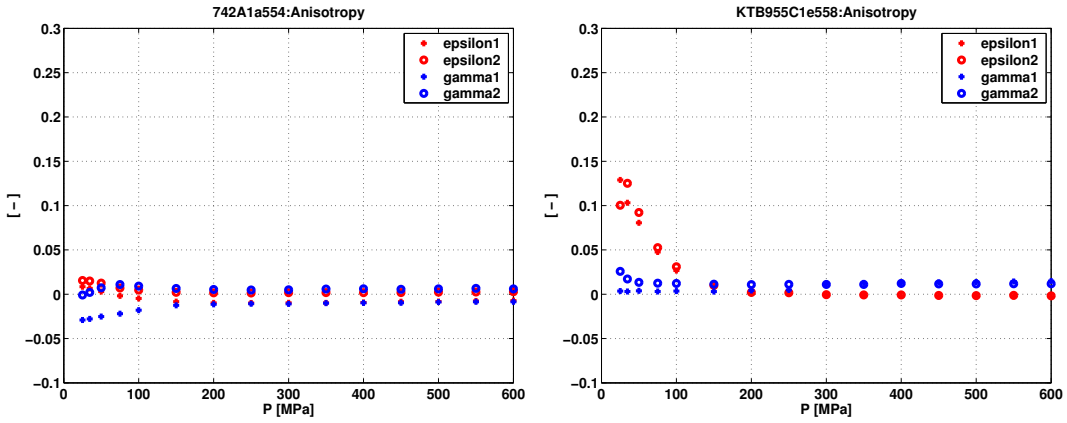

(a)

(b)

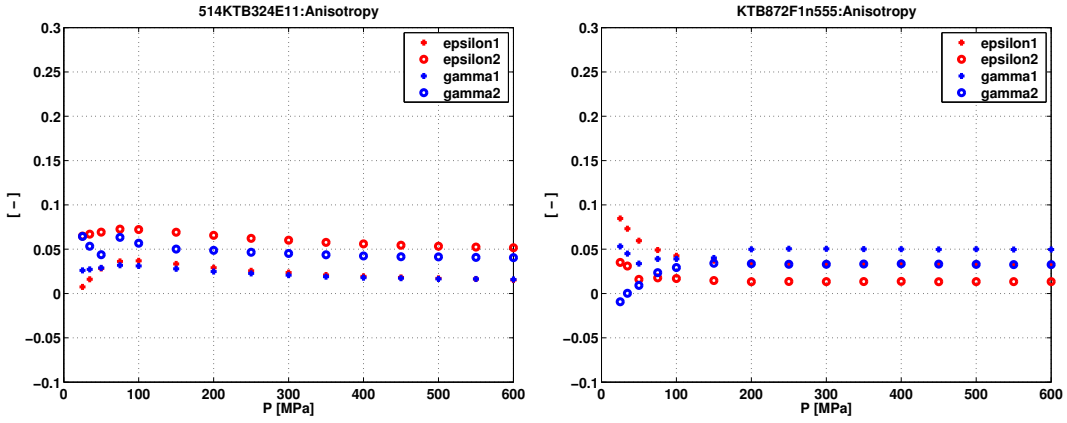

(c)

(d)

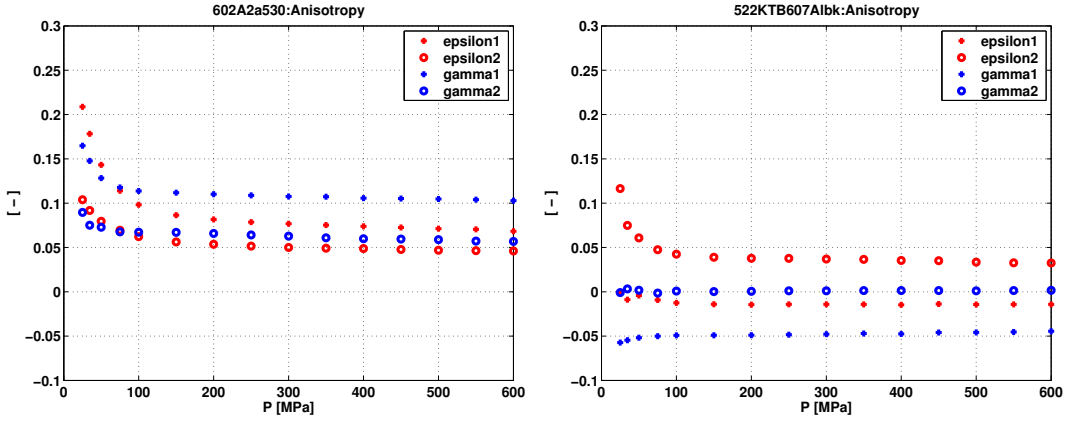

(e)

(f)

Figure 4.22: Tsvankin's parameters for KTB samples 742A1a554 (Fig. 4.22(a)), 955C1e558 (Fig. 4.22(b)), 514KTB324E11 (Fig. 4.22(c)), 872F1n555 (Fig. 4.22(d)), 602A2a530 (Fig. 4.22(e)), and 522KTB607Albk (Fig. 4.22(f)).

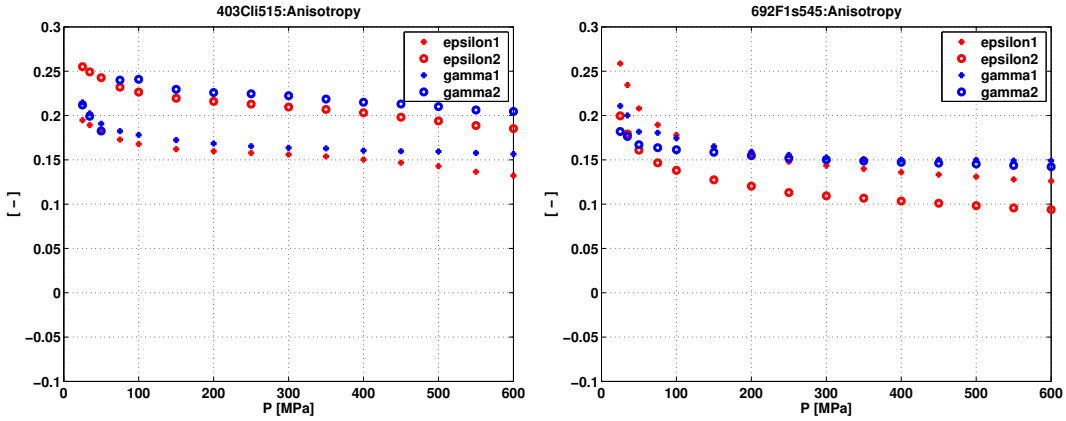

(a) (b)

Figure 4.23: Tsvankin's parameters for KTB samples 403Cli515 (Fig. 4.23(a)), 692F1s545 (Fig. 4.23(b)).

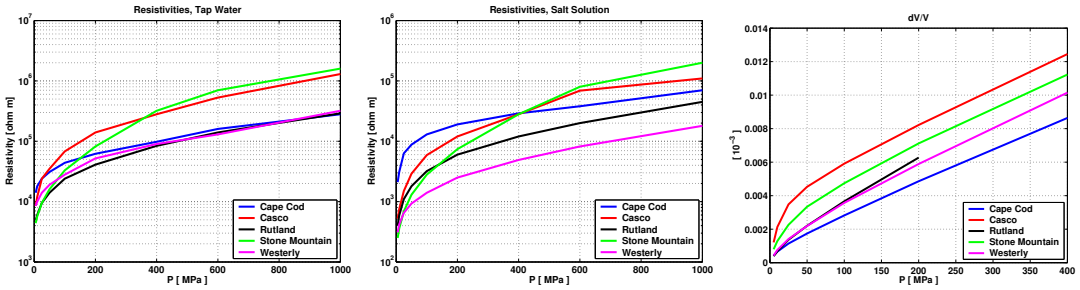

(a) (b) (c)

Figure 4.24: Resistivity of rock samples saturated with tap water (4.24(a)) and salt solution (4.24(b)) as well as bulk deformation of the samples (4.24(c)). Data from Brace *et al.* (1965).

Pressure dependent resistivity for the mentioned rocks saturated with tap water and salt solution are shown in Fig. 4.24(a) and 4.24(b), respectively, as well as strain data (Fig. 4.24(c)).

Figure 4.25 and 4.26 show a comparison between the observations and the fit results for Westerly and Casco granite (Fig. 4.27 and 4.28). It was possible to fit the bulk modulus (Fig. 4.25(a) and 4.27(a)) as well as the resistivity data - sample saturated with tap water (Fig. 4.25(b), 4.27(b)) and salt solution (Fig. 4.25(c), 4.27(c)) - quite well. The best fit parameters for the initial fits are listed in tab. 4.9.

As representative examples the best fit parameters for Cape Cod granodiorite and Casco granite are listed in tab. 4.10. Cape Cod stands for the worst agreement between theory and observation concerning a common D and Casco for the best (compare the D values in tab. 4.9). For Cape Cod we obtain a mean D of 0.043 $1/MPa$ (bulk modulus vs. resistivity of tap water saturated rock) and of 0.054 $1/MPa$ (bulk modulus vs. resistivity of rock saturated with salt solution). For Casco granite we found corresponding

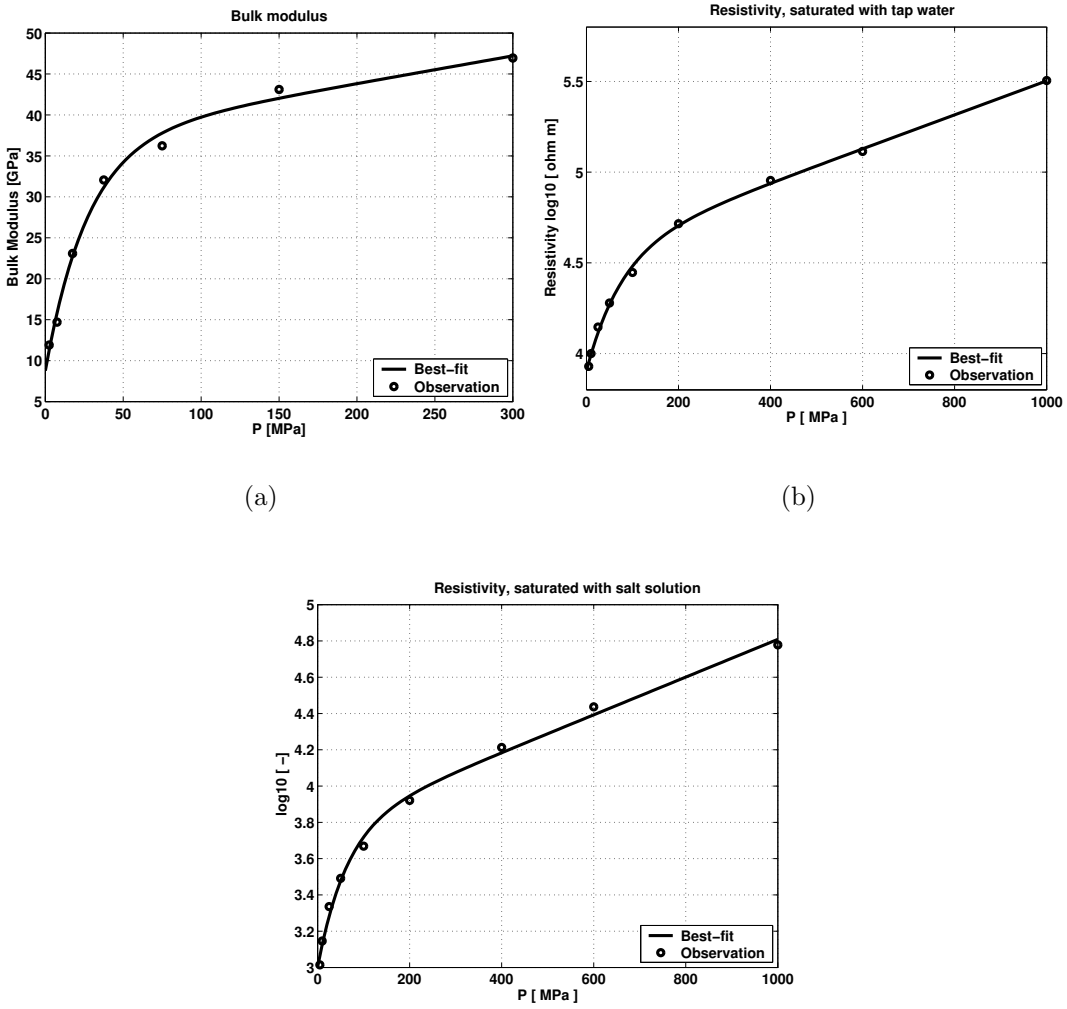

(a) (b)

(c)

Figure 4.25: Best fit of Westerly granite data. Bulk modulus (Fig. 4.25(a)), logarithmic bulk resistivity of rock saturated with tap water (Fig. 4.25(b)) and salt solution (Fig. 4.25(c)) were fitted separately with A, K, B, and D as fit parameters. Circles denote observations, lines the best fit.

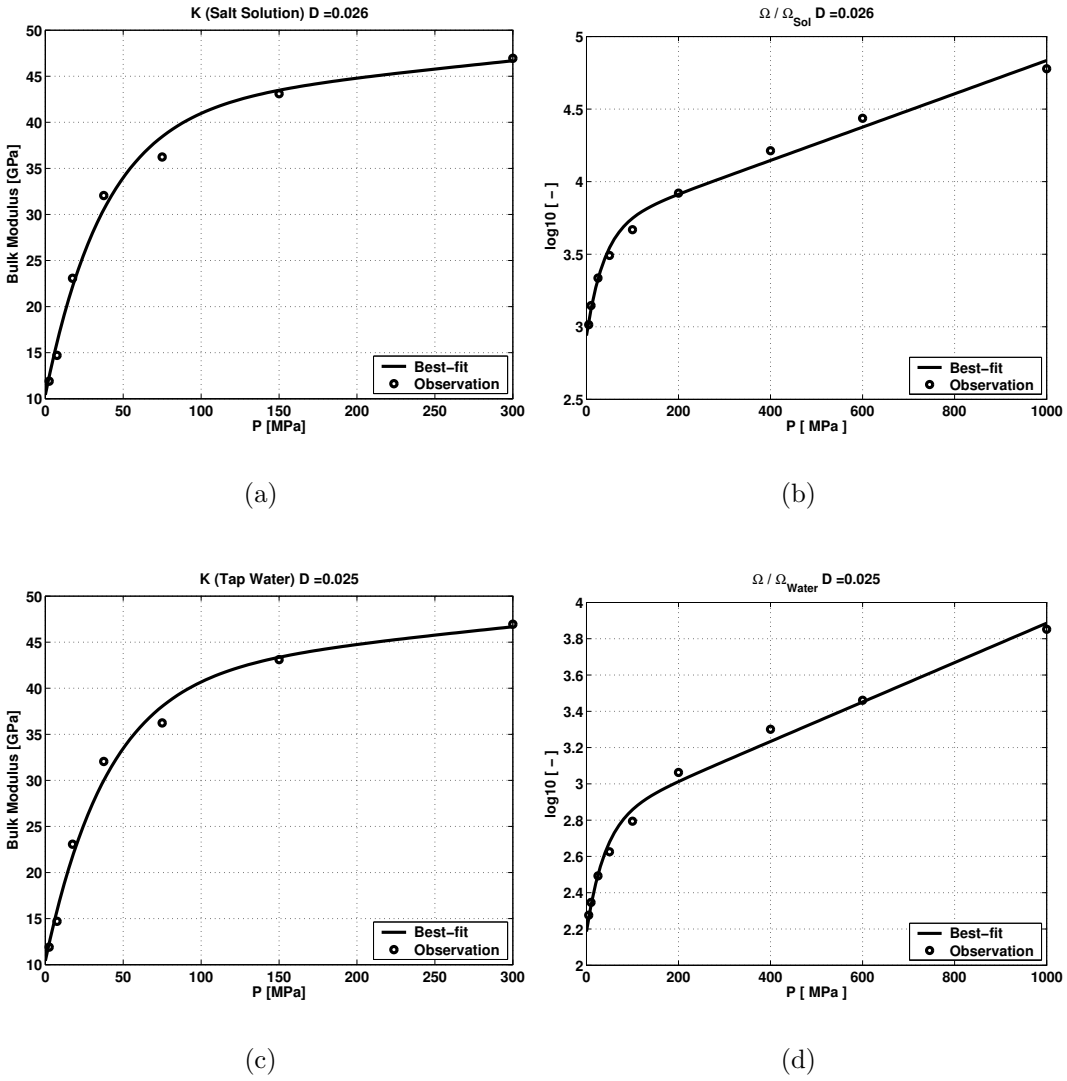

(a) (b)

(c) (d)

Figure 4.26: Second best fit of Westerly granite. Circles denote observations, lines best fit. Figure (4.26(a)) and (4.26(b)) show the repeated fit (see text for details) of bulk modulus and formation factor (salt solution saturated), respectively, with an averaged and fixed parameter D=0.026 MPa^{-1}. Figure (4.26(c)) and (4.26(d)) illustrate the result of the repeated fit with a fixed D=0.025 MPa^{-1} for bulk modulus and formation factor, respectively, where rock was saturated with tap water.

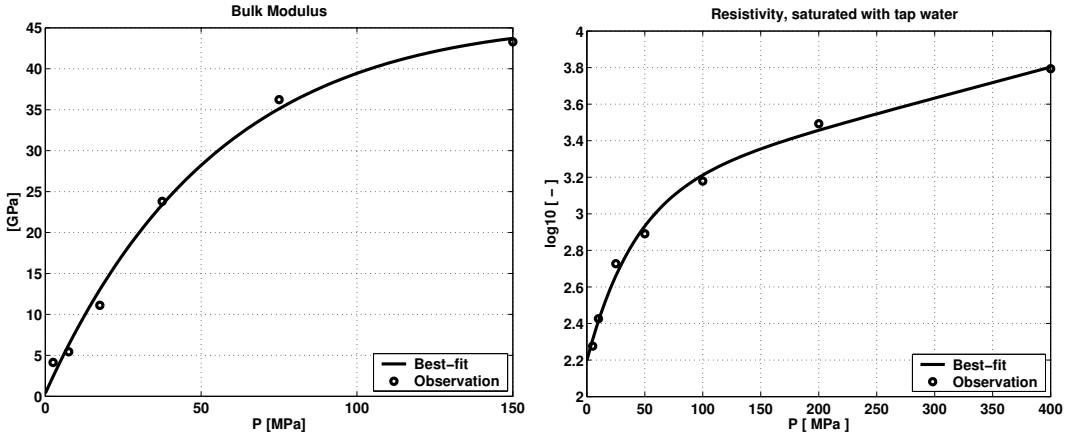

(a)

(b)

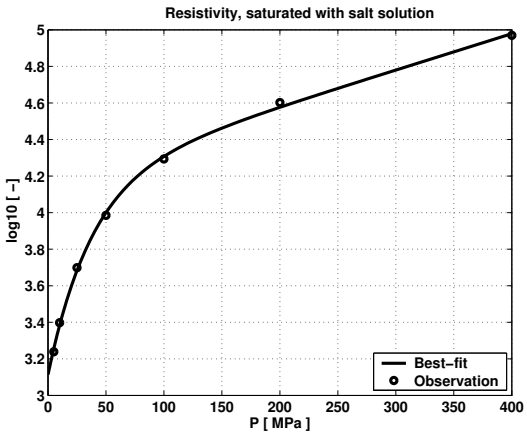

(c)

Figure 4.27: Casco granite data. Bulk modulus (fig. 4.27(a)), logarithmic bulk resistivity of rock saturated with tap water (fig. 4.27(b)) and salt solution (fig. 4.27(c)) were fitted separately with A, K, B, and D as fit parameters. Circles denote observations, lines the best fit.

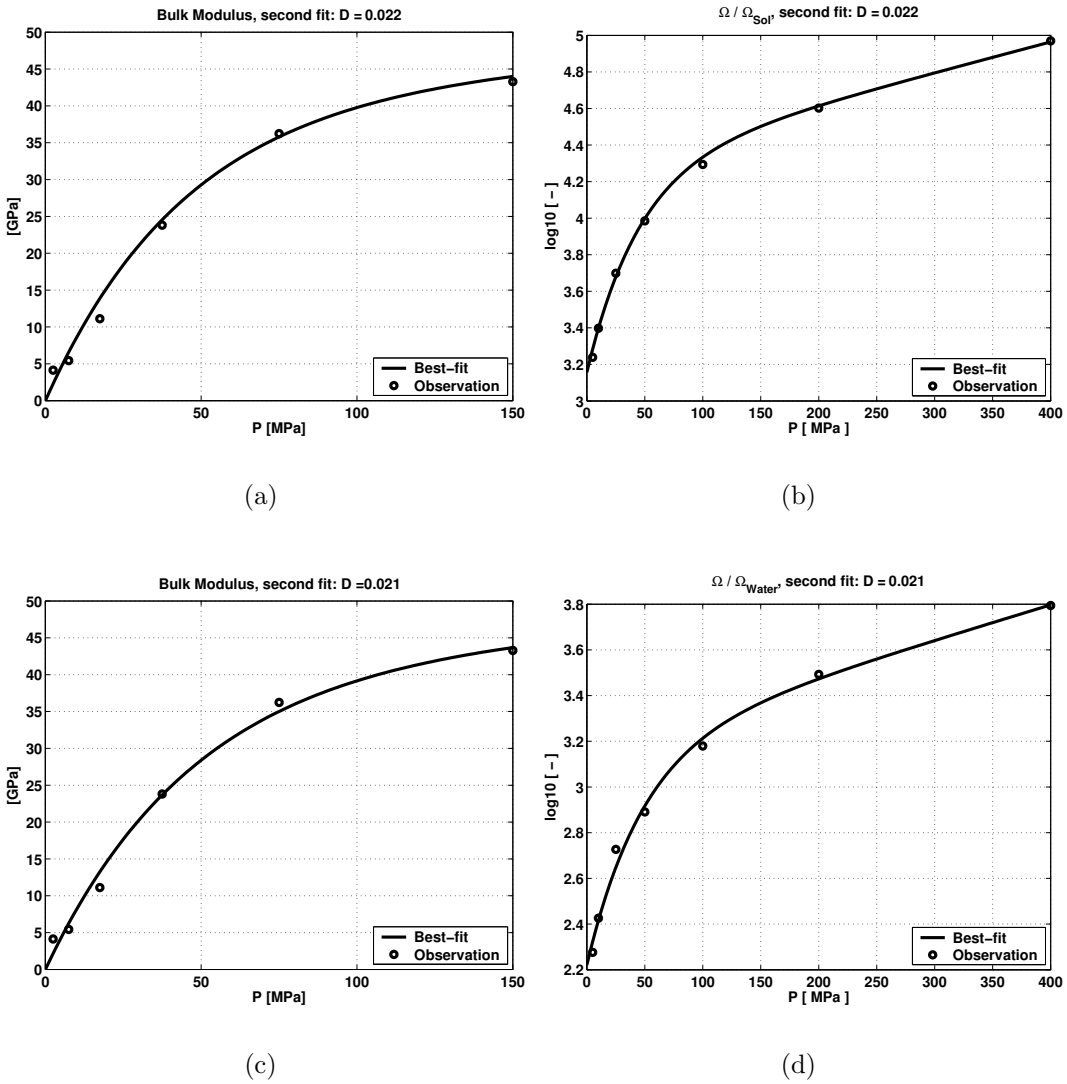

(a) (b)

(c) (d)

Figure 4.28: Second best fit of Casco granite data. Circles denote observations, lines best fit. Figure (4.28(a)) and (4.28(b)) show the repeated fit (see text for details) of bulk modulus and resistivity (salt solution saturated), respectively, with an averaged and fixed parameter D=0.022 MPa^{-1}. Figure (4.28(c)) and (4.28(d)) illustrate the result of the second fit for bulk modulus and resistivity (rock saturated with tap water), respectively, with D=0.021 MPa^{-1}

Table 4.9: Best fit parameters as obtained from fitting resistivity and dilatancy data obtained from Westerly and Casco granite. In the case of resistivity Ω units are [ohm m] for parameter A and B, [(ohm m) / MPa] for K, and [1/MPa] for D. Subscribes T and S denote saturation with tap water and salt solution, respectively. In the case of the bulk modulus K units are similar with [GPa] instead of [ohm m]. χ^2 is the sum of the squared deviations between the best fit model and the observations.

	Westerly			Casco		
Parameter	Ω_T	Ω_S	K	Ω_T	Ω_S	K
A	2.900	3.769	37.9	3.126	4.184	49.5
K	0.001	0.001	0.03	0.002	0.002	-0.01
B	0.648	0.766	28.3	0.928	1.070	49.2
D	0.014	0.016	0.036	0.024	0.027	0.017
χ^2	0.004	0.013	6.11	0.010	0.002	8.90

Table 4.10: Best fit parameter from second fit of Cape Cod and Casco data. Units are as mentioned in tab. 4.9.

	Westerly		Casco	
Parameter	Ω_T	K	Ω_T	K
D	0.025		0.021	
A	2.799	41.5	3.178	42.3
K	0.001	0.017	0.002	0.022
B	0.613	31.1	0.957	42.3
χ^2	0.016	10.97	0.011	10.70
Parameter	Ω_S	K	Ω_S	K
D	0.026		0.022	
A	3.687	41.5	4.291	42.3
K	0.001	0.017	0.002	0.022
B	0.748	31.1	1.134	42.31
χ^2	0.020	10.97	0.004	10.7

D values of 0.021 and 0.022.

For both examples presented above it was possible to fit static bulk moduli and logarithmic formation factors for water and salt solution saturated samples successfully. Moreover, the repeated fit of static bulk modulus and resistivity of the tap water saturated rock on the one hand and static bulk modulus and resistivity of salt solution saturated rock on the other hand revealed approximately the same value for D. This should be expectable as long as the bulk moduli of the saturating fluids are approximately equal and the experiments is conducted under drained conditions, i.e., as long as the pore pressure is kept constantly zero.

The quality of best fits for the remaining three samples was as good as for the mentioned two examples. In general, all logarithmic resistivity and dilatancy data could be modeled quite well. The best agreement between the different D values was obtained for Casco granite, as shown in tab. 4.10. Here, the first fit of the dilatancy

data delivered negative values for fit parameter K. However, a negative K does not seem to be a physically meaningful result. Since the absolute magnitudes of all K values for all samples are very small in comparison to the other parameters we assume that negative K values result rather from numerics of the fitting process than from any physical process occurring during compression. This might be interpreted in that way, that the closure of stiff porosity does not effect the mentioned stress dependencies at all and K could be eliminated from the fit equation when fitting bulk moduli data.

The good agreement between the parameter D for logarithmic formation factor and bulk modulus data seem to support our assumption that it is a universal characteristic for a given rock sample, not only for elastic moduli but also for transport properties like the electrical resistivity. This is, of course, limited to rocks where only electrolytic charge transport occurs. If these results are valid then the stress dependence of electrical resistivity in low porosity rocks is also mainly controlled by the elastic stress sensitivity and thus proportional to the inverse of an effective crack aspect ratio. In sediments, where the amount of stiff porosity is in general 2 orders of magnitudes higher than compliant porosity, the pressure dependence of electrical resistivity is controlled by the pressure dependence of stiff porosity. However, the universality of parameter D should also be valid in such rocks as long as the tensor of stress sensitivity has effectively only one independent entry.

4.6 Stress dependence of Poisson's ratio

In the following the stress dependence of ν for the dry rock sedimentary samples given by Freund (1992) as well as for the dry metamorphic KTB rocks will be considered in more detail. As already mentioned in section (3.5), in dry rocks the Poisson's ratio is usually constant for high stresses and increases with increasing effective stress in the low stress regime. As mentioned in section (3.5) the Poisson's ratio can theoretically take values between -1 and 0.5. Since the Poisson's ratio of the samples used here is always $0 < \nu < 0.35$ all plots are given in this range for an easy comparison of the different samples.

Figure (4.29) shows the confining stress dependent P- and S-wave velocities and Poisson's ratio for sample 140. The latter was calculated from the observed velocity data using eq. (3.67). P-wave velocity is more sensitive to increasing stress than S-wave velocity. Thus, the remarkable increase of ν with increasing stress shows the exponentially saturating behavior typical for the velocities, too. The dotted blue line in Fig. (4.29(a)) denotes Poisson's ratio as calculated from eq. (3.69) with best fit parameters obtained from velocity fits. For comparison, the solid blue line shows the resulting stress dependence of ν assuming $D_P = D_S$. Both regressions describe the observed stress dependence of ν quite well. Regarding the scatter of ν it is not obvious which regression fits better.

The stress dependence of ν in the case of sample 51 is small as also indicated by the stress dependence of P- and S-wave velocities (Fig. (4.30(a)) and (4.30(b)), respectively). The stress dependence of Poisson's ratio may even be approximated with a straight line. This indicates that the closure of compliant porosity is less dominant for the stress sensitivity of velocities. Carcione & Cavallini (2002) argues that rocks

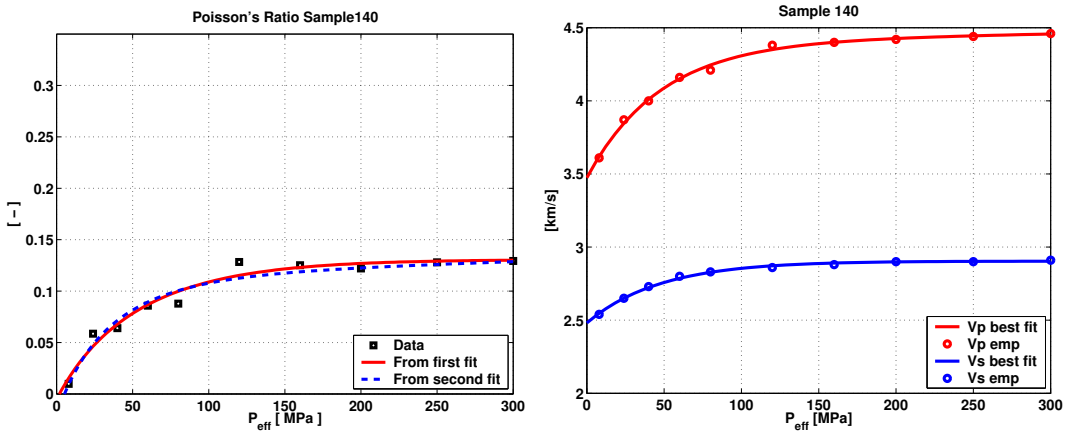

(a) (b)

Figure 4.29: Sample 140:(left) Poisson's ratio, calculated from observed velocities (black squares), calculated with DP = 0.019 and DS = 0.023 (dashed blue line), and a mean D = 0.021 (solid red line). (right) Observed (circles) P- (red) and S-wave (blue) velocities and best fit (lines) with D = 0.021 per MPa.

with mainly spherical voids show such a Poisson's ratio. However, since the stress sensitivity depends on θ_c rather than on the amount of stiff and compliant porosity, θ_c seems to be small and/or ϕ_{c0} is unusually small.

Sample 43 (see Fig.4.31) shows a different dependence of ν upon stress than the above mentioned examples. Up to approximately 70 MPa load ν typically increases. However, for higher stresses ν slightly decreases. This might result from measurement errors but could illustrate the influence of cracks on ν since the compliant porosity seems to be closed above approx. 100 MPa, as indicated by the more or less constant or slightly linearly increasing velocities above that stress level. As for the other examples Fig. (4.30(a)) also illustrates a comparison between ν calculated from first best fit parameters with different D values for P- and S-wave velocities (dotted blue line) and calculated from second fit with a common D = 0.021 per MPa. In this case, both curves show a distinct behavior above 60 MPa where the latter deviates from the data while the first describes the data exactly. This illustrates the stronger disagreement of fit parameter D obtained from first P- and S-wave velocity fit, regarding the disagreement for the two samples mentioned above. The deterioration of the regression due to the second fit of the data with an averaged D is not visible in the velocities. As shown in Fig. (4.31(b)) the regression of the velocity data with the averaged D parameter seems to be perfect.

In contrast to the previously discussed stress dependence of Poisson's ratio for the sandstone data given by Freund (1992) the following examples illustrate the ν as a function of stress obtained from saturated rocks, given by Eberhart-Phillips *et al.* (1989). In saturated rocks the strength of compliant porosity is enhanced which, in turn, increases the bulk modulus stronger than the shear modulus. As a consequence, ν is usually larger in saturated rocks and decreases with increasing applied stress (Carcione & Cavallini, 2002).

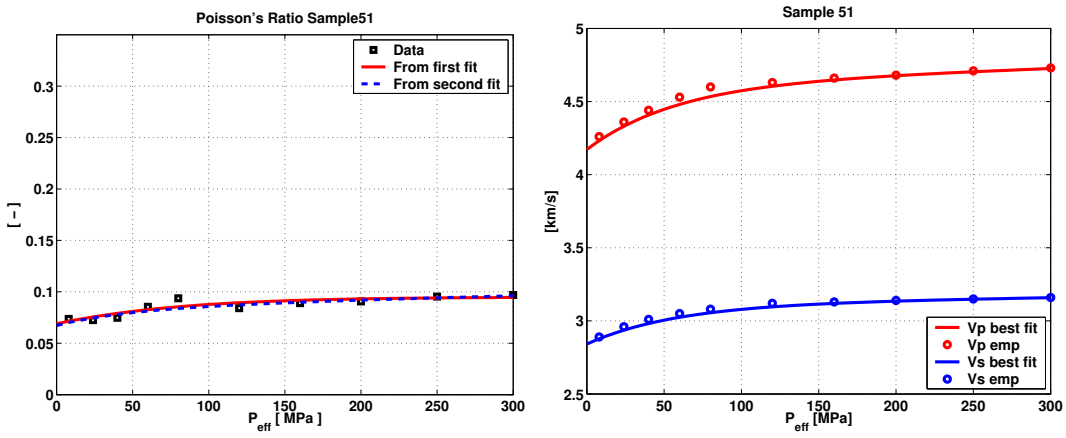

(a) (b)

Figure 4.30: Sample 51:(left) Poisson's ratio, calculated from observed velocities (black squares), calculated with DP = 0.017 and DS = 0.018 (dashed blue line), and a mean D = 0.017 (solid red line). (Right) Observed (circles) P- (red) and S-wave (blue) velocities and best fit (lines) with D = 0.017 per MPa.

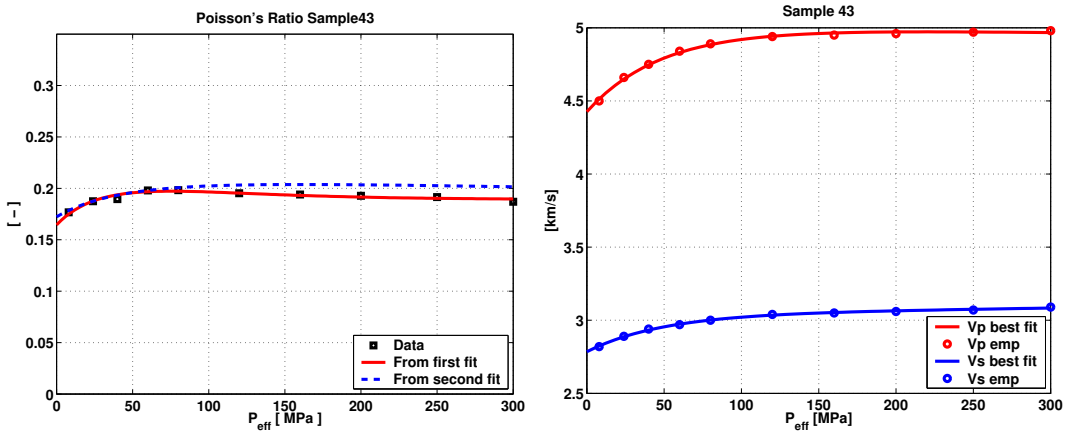

(a) (b)

Figure 4.31: Sample 43:(left) Poisson's ratio, calculated from observed velocities (black squares), calculated with DP = 0.024 and DS = 0.017 (dashed blue line), and a mean D = 0.021 (solid red line). (Right) Observed (circles) P- (red) and S-wave (blue) velocities and best fit (lines) with D = 0.021 per MPa.

Sample 51 (Fig. 4.32) represents an illustrative example for ν in saturated rocks. Poisson's ratio is higher than for the dry rocks mentioned before and decreases over the entire range of applied stress (Fig. 4.32(a)). This corresponds to P- and S-wave velocities which increase remarkably up to 200 MPa (Fig. 4.32(a)). Unfortunately, Eberhart-Phillips *et al.* (1989) give only best fit data, hence, a comparison of the regressions with observations is not possible. However, ν calculated from given best fit data (solid red line) and from refitted best fit data agree very well up to $\approx$ 200 MPa. Similar to the velocities, ν shows two different domains with respect to the slope of the stress dependence. For stresses below approx. 30 MPa ν decreases rapidly and non-linearly. For higher stresses the slope of the ν vs. stress relation is linear and more flat. This behavior may result from measurement errors in the very low stress regime or indicate the distinct sensitivity of ν to crack and compliant porosity closure. If the latter is true the bend in the relation might be understood as an indicator for stress magnitude where most cracks are closed.

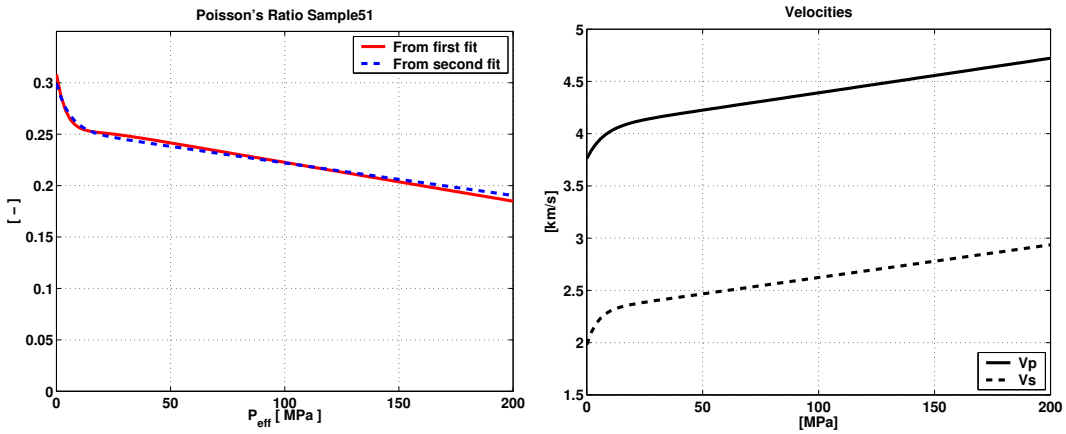

(a) (b)

Figure 4.32: Fig. (4.32(b)): Poisson's ratio calculated from Eberhart-Phillips et al. fit parameter (solid red line) and from refitted best fit parameters (dashed blue line.). Fig. (4.32(b)): P- and S-wave velocities calculated from best fit parameters (sample 51, saturated) given by Eberhart-Phillips *et al.* (1989).

The stress dependent Poisson's ratio of the KTB rocks was investigated in a similar manner. For each measurement direction one Poisson's ratio was calculated from P- and S-wave velocities. Therefore, a mean S-wave velocity was calculated from both measured S-waves for a given direction. Then, the Poisson's ratio was calculated from the best fit parameters of P- and S-waves obtained from the first and the second fit.

A comparison of the different stress dependent relations for sample 403Cli515 is given in Fig. (4.33). The stress dependence of Poisson's ratio is small in all directions. However, the absolute magnitudes of Poisson's ratio differ in all directions. Both theoretical approximations, obtained from best fit parameters of first and second fit, describe the observations quite well. They differ only slightly at approx. 50 MPa effective stress. If the interpretation is valid that the Poisson's ratio is a sensitive measure for a possible „isotropy" of the stress sensitivity tensor, then, the good agreement between both fit results and the data indicates that tensor of stress sensitivity of this

sample is effectively isotropic. This is remarkable, since the elastic properties of the sample seem to show an orthorhombic anisotropy (see Fig. 4.23(a)).

The same analyzis was done for KTB sample 955C1e558 (Fig. (4.34)). The Poisson's ratio in 1- and 2-direction is practically independent from stress ($\nu \approx 0.25$). In contrast, the Poisson's ratio in 3-direction shows a strong dependence upon stress, similar to the velocities. A comparison of the data to best fit approximations obtained from the best fit parameters of the first and fit shows that they differ stronger than for sample 403Cli515 at least in the 1- and 3-direction. However, taking measurement errors and the influence of averaging S-wave velocities into account both approximations describe the data well. In 2-direction both they completely coincide with the data.

Only KTB sample 522KTB607Albk shows a strong deviation of the Poisson's ratio calculated from first and second set of best fit parameters as illustrated in Fig. (4.35). Especially in the 1-direction the Poisson's ratio calculated from the second fit with a common parameter D does not match the measured data. This can also be found for the 2 direction, but here, the deviation decreases with increasing stress. However, in contrast to all other Poisson's ratios the approximation of the first fit deviates from the data with increasing stress. In the 3-direction the Poisson's ratio calculated from the best fit parameters of the second fit deviates from the data below 100 MPa. This is in contrast to the Poisson's ratio calculated from the best fit parameters of the first fit.

The stress dependent Poisson's ratio of sample 522KTB607Albk differs from all other samples. This might be understood as a hint that the tensor of stress sensitivity of this sample has a symmetry that does not correspond to one of an isotropic medium. However, this is in contrast to the practically stress independent anisotropy parameters of the sample as shown in Fig. (4.22(f)).

The analyzis of the stress dependent Poisson's ratio of the KTB rocks also indicates that the Poisson's ratio is a sensitive measure for a possible isotropic tensor of stress sensitivity. With only one exception, sample 522KTB607Albk, the Poisson's ratio seems to support that all considered KTB rocks show stress sensitivities of an isotropic medium, even the samples with a clear elastic anisotropy.

Most samples show a usually small deviations of the Poisson's ratios calculated from the fit parameters of the first and second fit below 100-150 MPa. This might be caused by measurement errors. It has to be taken into account that the measurements were conducted on cubic samples in a true-triaxial pressure vessel (see section (4.3) for details). Hence, it might be possible that the state of stress, especially for low effective stress, was rather quasi- than exactly isostatic.

4.7 Summary

In this chapter the stress dependence of various rock properties, i.e., seismic velocities, Poisson's ratio, anisotropy, and electrical resistivity of very different rock types was analyzed using the Stress Sensitivity Approach. This covers dry and saturated sedimentary and crystalline metamorphic rocks. It was possible to fit almost all P- and S-wave velocities of all samples very well. In this context, the main focus was to

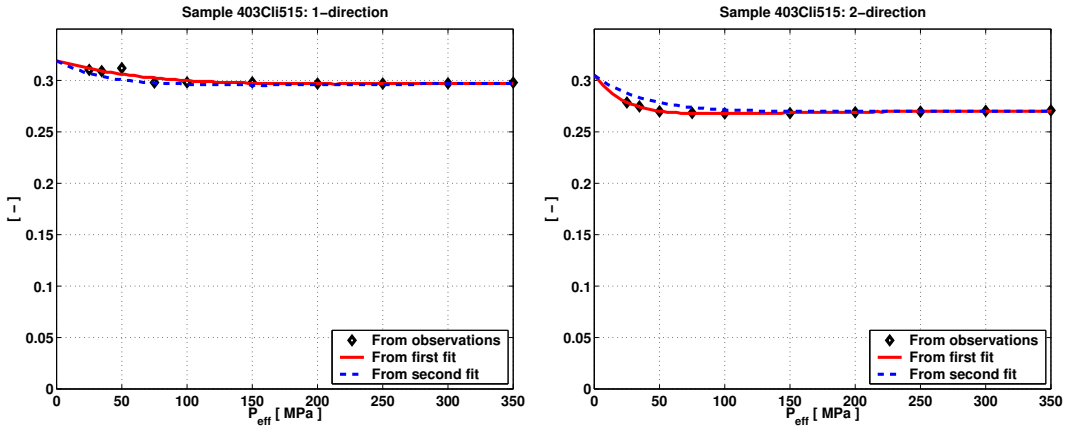

(a)

(b)

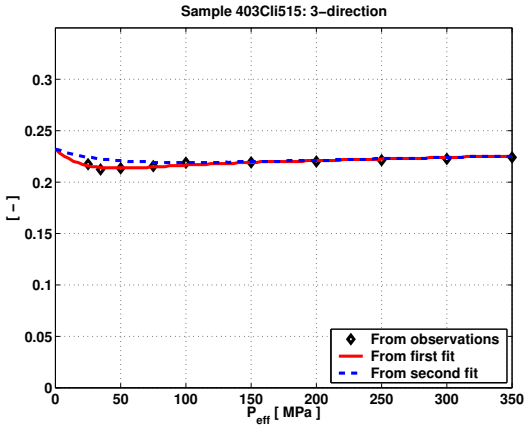

(c)

Figure 4.33: Stress dependent Poisson's ratio for KTB sample 403Cli515 in 1- (Fig. 4.33(a)), 2- (Fig. 4.33(b)), and 3-direction (Fig. 4.33(c)). Black diamonds indicate Poisson's ratio calculated from observed velocities. The blue and the red line denote Poisson's ratio calculated from best fit parameters obtained from first and second fit, respectively.

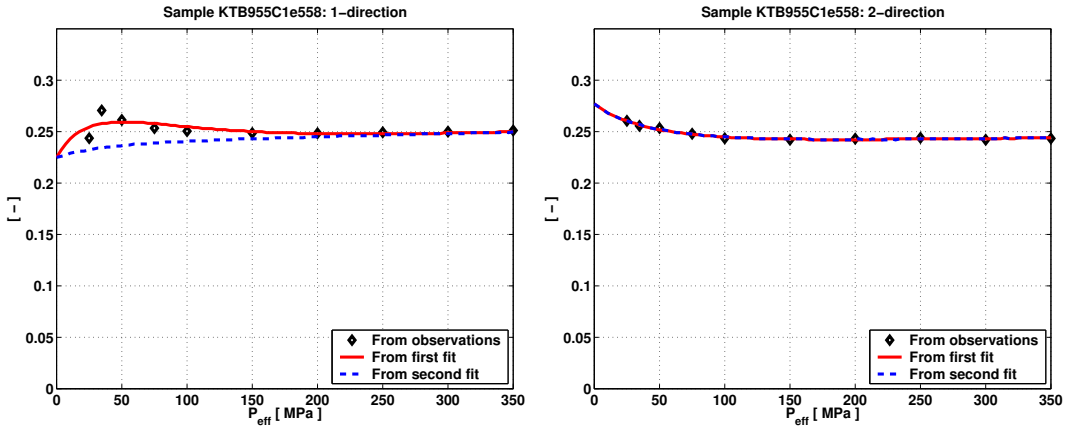

(a)

(b)

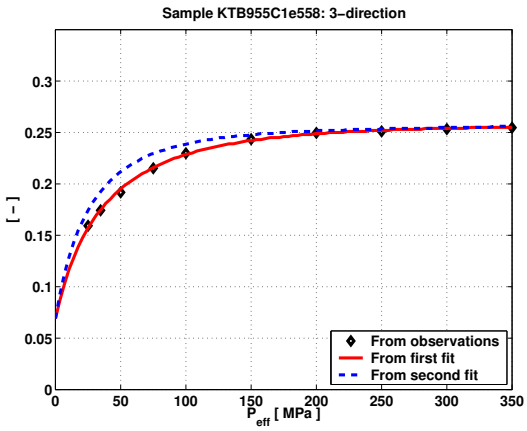

(c)

Figure 4.34: Stress dependent Poisson's ratio for KTB sample 955C1e558 in 1- (Fig. 4.34(a)), 2- (Fig. 4.34(b)), and 3-direction (Fig. 4.34(c)). Symbols and colors correspond to Fig. (4.33).

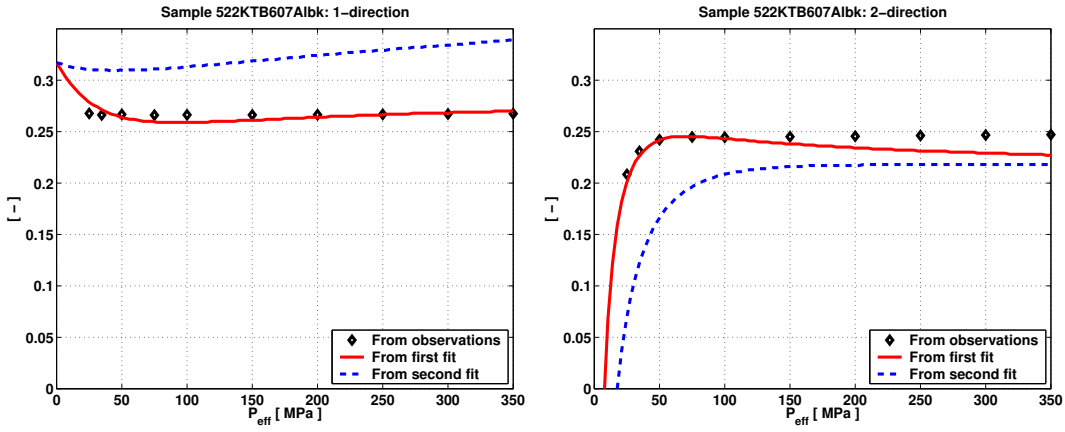

(a)

(b)

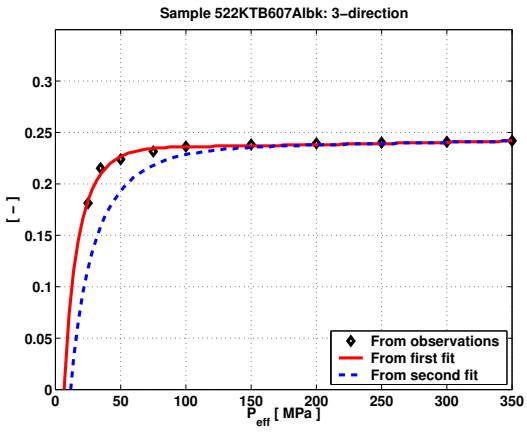

(c)

Figure 4.35: Stress dependent Poisson's ratio for KTB sample 522KTB607Albk in 1- (Fig. 4.35(a)), 2- (Fig. 4.35(b)), and 3-direction (Fig. 4.35(c)). Symbols and colors correspond to Fig. (4.33).

check, if there are rocks with a stress sensitivity tensor showing only one independent element. In this case, all velocities of a certain sample should have the same parameter D.

Even if rocks show exactly such a tensor of stress sensitivity it is not reasonable to expect that a regression of P- and S-wave velocity data directly gives the same parameter D. This is mainly caused by measurement errors as well as numerical artefacts introduced by the non-linear fit procedure. Thus, a two-step fit procedure was applied. In the first step a non-linear least squares fit was iteratively applied to the observed velocities. In the second step, the mean of all obtained parameters D of a given sample was calculated and used as a universal constant for the repeated fit of the data. This linearizes the fit equation in its parameters and enables a standard linear least squares fit. It was found, that it was possible to apply this procedure quite successfully to all samples, both isotropic as well as anisotropic. The accuracy of the second fit with a constant parameter D was always in the order of the first fit, sometimes slightly better, sometimes slightly less accurate. However, in any case, the second fit approximated the observed velocities very well.

A cross plot of DS vs. DP comprising the fit parameters of all sedimentary samples given by Eberhart-Phillips *et al.* (1989); Jones (1995) and Freund (1992) shows that the parameters, in fact, line up along DP = DS (Fig. 4.36(a)). The scatter of the data is caused by measurement errors as well as errors resulting from the first order approximations made in the derivation of the Stress Sensitivity Approach. The deviation from the postulated universality of parameter D seems to increase with the magnitude of D.

However, a least squares linear regression of the data reveals a coefficient of determination $R^2 = 0.82$ with respect to the regression line DS = 0.926DP + 0.002. This shows that the result of an effectively isotropic tensor of stress sensitivity, resulting in a universality of parameter D, is reasonable for many rocks.

This result was confirmed by analyzing the stress dependent anisotropy parameters for VTI rocks given by Lo *et al.* (1986) and the anisotropic rocks of the KTB. If the symmetry of the tensor of stress sensitivity corresponds effectively to the symmetry of an isotropic medium the anisotropy of the rocks should be independent from an applied isostatic load. This was, in general, found for the mentioned rocks.

However, it was also found that the stress dependence of Poisson's ratio is most sensitive to the deviations of the tensor of stress sensitivity from isotropy.

It was also shown that even the stress dependence of the logarithmic electrical formation factor can be formulated in terms of the Stress Sensitivity Approach. If the electrical resistivity of a rock can be described with Archies's law, the stress dependence of the rocks resistivity is also a function of pore space deformation. In contrast to the stress dependence of elastic properties, the stress dependence of electrical resistivity depends on the absolute magnitude of stiff and compliant porosity changes. Thus, the stress dependence of resistivity is usually assumed to be independent from stress in sedimentary rocks since the fractional part of the compliant porosity is negligible. However, in low porosity crystalline rocks, it was possible to describe the stress dependence of electrical resistivity and static bulk modulus with a universal parameter D.

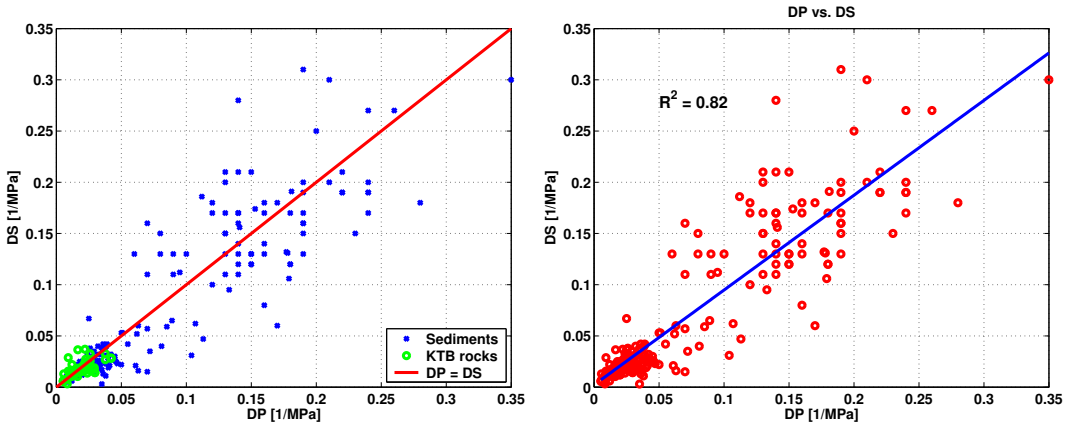

(a) (b)

Figure 4.36: DS vs. DP cross plot for all sedimentary (blue dots) samples from Eberhart-Phillips *et al.* (1989); Jones (1995); Freund (1992) and crystalline KTB rocks (green circles). The red line indicates DP = DS (Fig.4.36(a)). A linear least squares regression of DP vs. DS is shown in Fig.4.36(b) as blue line and the same data given in Fig.4.36(a) are illustrated as open red circles. The regression reads DS = 0.926DP + 0.002 with a coefficient of determination $R^2 = 0.82$.